Ingress of Li into solid electrolytes: cracking and sparsely filled cracks

D. Mukherjee[a], S. Hao[b,c], P.R. Shearing[b,d], R.M. McMeeking[e], N.A. Fleck[a,d], and V.S. Deshpande[a,d*]

[a] *Department of Engineering, University of Cambridge, Cambridge CB2 1PZ, UK*
[b] *Electrochemical Innovation Lab, Department of Chemical Engineering, University College London, London WC1E 7JE, UK*
[c] *Institute of New Energy Material Chemistry, School of Materials Science and Engineering, Nankai University, Tianjin 300021, China*
[d] *The Faraday Institution; Quad One, Harwell Science and Innovation Campus, Didcot, UK*
[e] *Department of Mechanical Engineering & Materials Department, University of California, Santa Barbara CA 93106, USA*

submitted to *Small Structures*

Abstract

The growth of Li dendrites in a solid electrolyte is commonly idealised by a pressure filled crack. Recent observations in both garnet and sulphide electrolytes show that sparsely filled cracks exist prior to shorting of the cell thereby invalidating this assumption. Here we develop a variational principle that uses the Onsager formalism to couple Li deposition into the crack, elastic deformation of the electrolyte and cracking of the electrolyte with the electrochemical driving forces and dissipation within the electrolyte and interfaces. Consistent with observations we show that Li ingress and cracking occur together for garnet electrolytes, but the cracks are sparsely-filled. This sparse filling is a direct consequence of the mismatch between the elastic opening of the cracks and the deposition of Li into the cracks across the crack flanks. An increase in the resistance of Li ingress into the tips of Li filaments results in the crack propagating ahead of the Li filaments, as observed for sulphide electrolytes. In such cases the cracks are largely dry. Our results provide a framework to model Li ingress into solid electrolytes and explain why the observations are qualitatively so different from dendrites in liquid electrolytes.

Keywords: Ceramic separator, solid-state battery, Lithium dendrite, variational principle.

* Corresponding author. E-mail address: vsd20@ cam.ac.uk

1. Introduction

Solid-state batteries with lithium (Li) metal anodes offer the possibility of enhanced energy density and enhanced safety. These solid-state batteries typically employ ceramic electrolytes such as the Li stuffed garnet $Li_7La_3Zr_2O_{12}$ (LLZO) or sulphides such as Argyrodite (Li_6PS_5Cl) or LPS ($Li_2S - P_2S_5$) [1-3]. However, fully dense ceramic electrolytes can suffer from short-circuits due to Li filament/dendrite penetration from the Li metal anode when the current density of the anode exceeds a critical current density (CCD) [1,4-6]. It is desirable to enhance the CCD of a solid-state battery (SSB) in order to allow for faster charging of electric vehicles, for example.

Several factors influence the CCD. For example, the CCD decreases with increasing grain size of the ceramic electrolyte [7-9] and also decreases with increasing electrolyte/electrode interface ionic resistance [9-12]. Recent observations [13-16] suggest that dendrites grow in the vicinity of voids in Li anodes at the electrode/electrolyte interface. These voids form during the stripping phase, and the required current to grow these voids is typically much less than the CCD for dendrite propagation. These observations of void formation in the metal electrode and associated Li metal penetration are very general and qualitatively similar observations have also been reported for Na^+/beta-alumina systems [17].

The assessment of dendrite propagation in ceramic electrolytes has, to-date, been restricted to modelling them as pressurised cracks [18-23]. This concept was first used to explain dendrite formation in Na^+/beta-alumina systems [24] and has been extended more recently to Li dendrite formation in garnet electrolytes [18,20-21]. While details of the models differ all assume that the Na or Li have a sufficiently low shear strength that they behave as a fluid, and consequently crack propagation is driven by the high fluid pressure generated by the electric overpotential across the crack flanks [22,25-26]. In a slightly different vein, Shishvan et al. [27-28] assumed that dendrites possess the same geometry as parallel sided-edge dislocations, with penetrating Li metal forming the "extra half-plane" of the edge dislocation. A defining feature of all these models is that the crack advance and Li/Na metal deposition within the crack proceed in unison: the metal completely fills the crack and the plating out of metal at the crack tip drives crack propagation.

The idealisation of a dendrite as a pressurised crack or a macro-dislocation is called into question by recent X-ray computed tomographic (X-ray CT) observations and associated measurements. Bruce and co-workers [29] reported X-ray CT observations which clearly show that cracks propagate in Argyrodite-type LPS (Li_6PS_5Cl) electrolytes as empty, dry cracks: Li metal is only present at the crack mouth near the plating electrode. They reported that a through-crack develops after 25 minutes in an electrolyte of thickness 1 mm when the imposed current is $i_\infty = 1.5\ \mathrm{mAcm^{-2}}$, but the cell does not immediately short. This was subsequently confirmed for LPS electrolytes by the X-ray CT observations of Shearing and co-workers [30] reproduced in Fig. 1a: the electrolyte has cracked through its thickness, but Li (shaded in red) is present only near the plating electrode. In fact, at the time of through-cracking of the electrolyte, only about 20% of the volume of the crack is occupied by Li. In contrast, for the case of an LLZO electrolyte, through-cracking and shorting occur almost simultaneously (and at a shorting time on the order for 2-10 mins which is much less than that for LPS [10]). This suggests that the above-described pressurised crack models are applicable for LLZO. However, using nano X-ray CT methods Shearing and co-workers [31] observed that, while Li penetration and cracking occur approximately in unison for LLZO, the cracks within LLZO are only sparsely filled (Fig. 1b). Collectively, these observations suggest that there remains a

lack of understanding of the mechanisms by which dendrites propagate into solid electrolytes; current modelling frameworks are not reconciled with experimental observations.

All models to-date employ a quasi-equilibrium approximation which governs the pressure/state of the Li within the crack. This assumption inherently results in the pressurised and filled crack prediction which seems inconsistent with observations. Here we shall use the Onsager formalism to develop a non-equilibrium, kinetic framework for the penetration of Li into ceramic electrolytes. The shape, filling and propagation of the crack by Li filaments/deposits are natural outcomes of the solution of the variational principle. We shall show that, unlike in liquid electrolytes where elasticity of the electrolyte plays no role, sparsely filled cracks are to be expected due to the mismatch between the elastic opening of the crack and the electrochemical forces that govern the filling of cracks.

2. Problem definition and a variational principle for crack growth

The penetration of Li into Li stuffed ceramic single-ion conductor electrolytes occurs from the Li metal electrode that is being plated. There exists significant controversy in the literature on the geometry of the dendrite/Li filament (is it a crack or a dislocation-like defect?) and whether the fractured electrolyte is fully filled with Li or not. Here, we shall develop a variational principle where the geometry of the dendrite/crack and the extent of filling are outcomes of the coupled electro-mechanical kinetics. The key outcomes of the analysis will include: (i) the conditions under which dendrites/cracks grow and (ii) the mode of growth of the dendrites/cracks. For consistency of terminology throughout this study we shall refer to the defect within the electrolyte as a crack and the Li within this crack as the Li filament. We do this to avoid confusion with the term dendrite which typically has been used to describe a defect that is fully filled with Li.

In line with many experiments that investigate crack growth in solid electrolytes, we consider a symmetric cell as shown in Fig. 2a with an external power source imposing a voltage difference Φ_p between the two electrodes. A pre-existing crack of length a_0 in the single-ion conductor electrolyte is assumed to emanate from the interface of the plating Li electrode (inset of Fig. 2a) and we develop a kinetic framework for investigating the response of this cell in terms of the growth of this pre-existing crack. We shall make two simplifying assumptions that are commonly employed for problems of this type:

(i) The electrolyte remains electroneutral such that every Li^+ cation is paired with an immobile anion within the single-ion conductor electrolyte. Thus, the Li^+ occupancy in the electrolyte is spatially uniform and flux is driven purely by the electric potential gradient.

(ii) The molar volume Ω_e of Li within the electrolyte is assumed to be zero [22, 27] because the Li in Li-stuffed ceramic electrolytes lies within a rigid ceramic skeleton that does not deform upon removal/addition of a Li atom.

In addition, it will be shown that the Li filaments within the cracks are less than 100 nm in thickness. Recent micro-pillar compression tests [32-34] suggest that Li pillars in the micron length-scale have a uniaxial yield strength σ_Y above 100 MPa. Direct measurements [35] of stresses in the electrolytes around cracks also suggest stresses on the order of 150 MPa. Taken together, this strongly suggests that Li within the crack is much stronger than bulk Li that creeps at a stress on the order of 1 MPa at room temperature [33]. Given the high stresses that Li filaments can sustain within cracks, we shall idealise the Li within the filaments as rigid.

Our aim is to analyse the growth of cracks and Li filaments within the electrolyte and to do so we define a system that occupies a domain $\mathcal{V}$, see Fig. 2a. This system excludes the external power supply but encompasses the entire electrolyte volume $\mathcal{V}_{\mathrm{SE}}$ and an infinitesimal layer of each electrode. Both metal electrodes are maintained at fixed electrical potentials by the external power supply and this sets known boundary conditions for the system being analysed. While this is the simplest system that can be analysed for investigating the growth of cracks, it is nevertheless a complex open system with fluxes of Li^+ ions across left and right boundaries of the system that are adjacent to the stripping and plating electrolyte/electrode interfaces $\mathcal{S}_S$ and $\mathcal{S}_P$, respectively, a change in the total Li content in the system as the Li filaments grows due to Li^+ ions being deposited into the crack, a net flux of electrons from the plating electrode to neutralize the Li^+ ions being deposited into the crack, and storage of elastic energy within the electrolyte associated with opening of the crack.

2.1 Brief description of the variational principle

Here we briefly describe the salient features of the variational principle with full details and mathematical derivations provided in Supplementary section S1. The kinetic variational principle makes use of the Onsager [36-37] formalism wherein the rate of loss of potential energy $\dot{\Pi}$ of the system drives the dissipation within the system. We treat the electroneutral single-ion conductor electrolyte as an isotropic linear dielectric with permittivity $\mathcal{E}_{\mathrm{SE}}$ and a conductivity κ for Li^+ ions. The electrolyte is also an isotropic linear elastic solid with shear modulus G and Poisson's ratio ν such that the stiffness tensor is $\mathbb{C}_{ijkl} = 2G\nu\delta_{ij}\delta_{kl}/(1-2\nu) + G(\delta_{ik}\delta_{jl}+\delta_{il}\delta_{jk})$, where δ_{ij} is the Kronecker delta and the stress σ_{ij} is related to the strain $\varepsilon_{ij} \equiv (u_{i,j}+u_{j,i})/2$ via $\sigma_{ij} = \mathbb{C}_{ijkl}\varepsilon_{kl}$ where u_i is the displacement field within the electrolyte. While the formulation is general and can be employed for a three-dimensional (3D) system with an arbitrary crack shape, here for simplicity we shall describe the formulation in a two-dimensional (2D) plane strain setting in the $x_1 - x_2$ plane with a crack growing in the x_1 −direction constrained to remain straight. Consider the system at a general time t such that a crack of length a and Li filament of length ζ exists within the electrolyte of thickness L and width W, as shown in Fig. 2a. Initially, at $t = 0$, the filament is of infinitesimal thickness and equal to the initial crack length a_0, i.e., $\zeta = a_0$. The voltage difference Φ_{p} is imposed at $t = 0$. The origin of the co-ordinate system is located at the mouth of the crack on the electrolyte/plating electrode interface and the x_1 −direction is perpendicular to the interface as shown in Fig. 2a. We shall assume that an electron-conducting pathway always exists over the entire length of the filament.

Contributions to the rate of change $\dot{\Pi}$ of a potential energy arise from: (i) the rate of change $\dot{N}_{\mathrm{Li}}$ of Li content within the system; (ii) the rate of change of electrical energy associated with the electric field E_i and electric displacement D_i where $D_i = \mathcal{E}_{\mathrm{SE}}E_i$, (iii) the current density j_i of Li^+ ions across the left and right system boundaries $\mathcal{S}_{\mathrm{L}}$ and $\mathcal{S}_{\mathrm{R}}$ shown in Fig. 2a and the current density j_i^{el} of electrons from the plating electrode; (iv) the rate of change $\dot{U}_{\mathrm{elas}}$ of elastic energy of the electrolyte and (v) the changes in the surface energy due to fracture of the electrolyte in terms of the fracture energy γ_{SE} and the adhesion energy γ_{adh} associated with the formation of new Li/electrolyte interfaces on the crack flanks. Then $\dot{\Pi}$ follows as (Supplementary section S1.3)

$$\dot{\Pi} = \dot{N}_{\mathrm{Li}}\mu_0 - \int_{\mathcal{V}} D_i\dot{E}_i d\mathcal{V} - \int_{\mathcal{S}_{\mathrm{T}}\cup\mathcal{S}_{\mathrm{B}}} D_i n_i \dot{\varphi} d\mathcal{S} + \dot{U}_{\mathrm{elas}} - \int_{\mathcal{S}} T_i\dot{u}_i\, d\mathcal{S} + \frac{1}{F}\int_{\mathcal{S}_{\mathrm{L}}} \mu_{\mathrm{Li}^+} j_i n_i\, d\mathcal{S} + \frac{1}{F}\int_{\mathcal{S}_{\mathrm{R}}} \mu_{\mathrm{Li}^+} j_i n_i\, d\mathcal{S} - \frac{1}{F}\int_{\mathcal{S}_{\mathrm{L}}} \mu_{el} j_i^{\mathrm{el}} n_i\, d\mathcal{S} - 2\gamma_{\mathrm{adh}}\dot{\zeta} + 2\gamma_{\mathrm{SE}}\dot{a}, \tag{1}$$

where μ_{el} and μ_{Li^+} are the chemical potentials of the electrons and Li^+ ions, respectively that leave/enter the system at electrode/electrolyte interfaces with outward unit normal n_i, μ_0 is the chemical potential of Li metal and F is the Faraday constant. Note that boundary integrals over the top and bottom free surfaces of the electrolyte $\mathcal{S}_{\text{T}}$ and $\mathcal{S}_{\text{B}}$ are included as D_i is specified on these surfaces while tractions specified over the entire surface $\mathcal{S} \equiv \mathcal{S}_{\text{L}} \cup \mathcal{S}_{\text{B}} \cup \mathcal{S}_{\text{R}} \cup \mathcal{S}_{\text{T}}$ of the system. Mass conservation dictates that

$$\int_{\mathcal{S}_{\text{L}}} j_i n_i \, d\mathcal{S} \; + \; \int_{\mathcal{S}_{\text{R}}} j_i n_i \, d\mathcal{S} \; = \; - \dot{N}_{\text{Li}} F, \tag{2}$$

while the requirement that the system remains charge neutral relates $\dot{N}_{\text{Li}}$ to the electron flux via

$$\int_{\mathcal{S}_L} j_i^{\text{el}} n_i \, d\mathcal{S} \; = \; \dot{N}_{\text{Li}} F. \tag{3}$$

In order to set up the Onsager principle, we also need to consider the sources of dissipation in the system and thereby define a dissipation potential $\mathcal{D}$. The four sources of dissipation within the system are: (i) Li^+ flux through the solid electrolyte of conductivity κ, (ii) the resistance Z_0 for the Li^+ flux across the electrode/electrolyte interfaces, (iii) the resistance Z_f for the Li^+ flux across the crack flank and (iv) the resistance R_{Tip} for Li^+ to acquire an electron at the tip of the Li filament as it forms a new Li/electrolyte interface on the crack flanks; see Fig. 2b. Consequently, the dissipation potential is defined by (Supplementary section S1.3)

$$\mathcal{D} \; = \frac{1}{2}\left[\frac{1}{\kappa}\int_{\mathcal{V}_{\text{SE}}} j_i j_i \, d\mathcal{V} \; + \; Z_0 \int_{\mathcal{S}_{\text{P}}} j^2 d\mathcal{S} + \; Z_0 \int_{\mathcal{S}_{\text{S}}} j^2 d\mathcal{S} + \; Z_f \int_{\mathcal{S}_{\Gamma}} j^2 d\mathcal{S} + 2R_{\text{Tip}} J_{\text{Tip}}^2 \right], \tag{4}$$

where $j = j_i n_i$ and $\mathcal{S}_{\Gamma}$ is the portion of the crack flanks over which the Li filament is present (inset of Fig. 2a) with n_i the outward unit normal to the electrolyte. In addition, J_{Tip} is the Li^+ current to the tip of the Li filament through each of the two crack flanks (symmetry dictates that the currents across the two flanks are equal) while conservation of Li dictates that the filament extends by a rate $\dot{\zeta} = 2J_{\text{Tip}}/(F\rho_{\text{m}}\delta_{\text{Tip}})$ where ρ_{m} is the molar density of Li and δ_{Tip} is the crack opening at the tip of the filament (inset of Fig. 2a). Note that Z_0 and Z_f are assumed to be constants, implying a linearized form of Butler-Volmer kinetics across the electrode/electrolyte interfaces and the crack flanks.

The rate of change of potential energy (1) is combined with the dissipation potential (4) to define an augmented potential $\dot{\Psi} = \dot{\Pi} + \mathcal{D}$ in terms of the independent field variables ($\check{u}_i, \dot{a}$, $j_i, J_{\text{Tip}}, \dot{\varphi}$) where φ is the electric potential and, $\check{u}_i$ is the time derivative of the displacement field at constant crack length as defined in Supplementary section S1.3. The Onsager principle [36] demands that the system evolves such that the fields satisfy $\delta\dot{\Psi} = 0$ at every instant. This requirement delivers the strongly coupled electro-mechanical governing partial differential equations and associated boundary conditions for the problem as derived in Supplementary section S1.3.

The governing equation for the electric field within the electrolyte $\mathcal{V}_{\text{SE}}$ is the electroneutral Gauss law given by $\hat{\varphi}_{,ii} = 0$ where $\hat{\varphi} = \varphi + \mathcal{U}$ and $\mathcal{U}$ is the open circuit potential between the electrolyte and Li metal. The boundary conditions associated with this Laplace equation are $D_i n_i = j_i n_i = 0$ on the lateral boundaries $\mathcal{S}_{\text{T}}$ and $\mathcal{S}_{\text{B}}$ (Fig. 2a) where $j_i = -\kappa\hat{\varphi}_{,i}$ while the flux of Li^+ through the electrode/electrolyte interfaces satisfies

$$j_i n_i \; = \; \frac{\hat{\varphi} - \Phi_{\text{P}}}{Z_0} \;\; \text{on} \;\; \mathcal{S}_{\text{S}} \qquad \text{and} \qquad j_i n_i \; = \; \frac{\hat{\varphi}}{Z_0} \;\; \text{on} \;\; \mathcal{S}_{\text{P}} \, . \tag{5}$$

By contrast, on the crack flank $\mathcal{S}_\Gamma$ where the Li filament is present, the flux boundary conditions involve the tensile stress σ_n across the interface via

$$j_f \equiv j_i n_i = \frac{1}{Z_f}\left(\hat{\varphi} + \frac{\sigma_n}{F\rho_{\mathrm{m}}}\right), \tag{6}$$

where n_i is the unit normal to the crack flank pointing into the crack. This boundary condition couples the solution of the electric field within the electrolyte to the mechanical problem. In addition, the electric field/potential within the electrolyte needs to admit a current sink of magnitude

$$J_{\mathrm{Tip}} = \frac{1}{R_{\mathrm{Tip}}}\left[\hat{\varphi}_{\mathrm{Tip}} + \left(\frac{2\gamma_{\mathrm{adh}}}{F\rho_{\mathrm{m}}\delta_{\mathrm{Tip}}}\right)\right], \tag{7}$$

at the Li filament tip of thickness δ_{Tip} located at ζ (Fig. 2b): this current sink lengthens the Li filament. Here, $\hat{\varphi}_{\mathrm{Tip}}$ is the value of $\hat{\varphi}$ in the vicinity of the filament tip within the electrolyte. This boundary condition requires special consideration as the existence of the sink implies a singularity in $\hat{\varphi}$ and a superposition methodology is used to solve for this singularity as detailed in Supplementary section S2.

Similarly, $\delta\dot{\Psi} = 0$ delivers the mechanical balance laws within the electrolyte, viz. the static equilibrium equation $\sigma_{ij,j} = 0$ along with the associated boundary conditions. These boundary conditions are: (i) the crack opening displacement δ_{Li} at time t along $\mathcal{S}_\Gamma$ is given by mass conservation as

$$\delta_{\mathrm{Li}}(x_1, t) = \frac{2}{F\rho_{\mathrm{m}}}\int_{\tau(x_1)}^{t} j_f\,(x_1, t')\,dt', \tag{8}$$

where j_f follows from (6) and $\tau(x_1)$ is the time at which the filament tip ζ is first located at x_1 and (ii) on all other electrolyte boundaries, i.e. $\mathcal{S}_{\mathrm{S}}, \mathcal{S}_{\mathrm{P}}, \mathcal{S}_{\mathrm{T}}, \mathcal{S}_{\mathrm{B}}$ and the crack flank $\mathcal{S}_{\mathrm{C}}$ where the Li filament is absent the tractions vanish such that $T_i = 0$. Additionally, $T_1 = 0$ over $\mathcal{S}_\Gamma$ (i.e., zero shear tractions between the Li filament and the electrolyte). The solution of $\sigma_{ij,j} = 0$ with these boundary conditions delivers the mechanical fields within the electrolyte for a given crack length a. It is emphasised that this mechanical solution requires a solution coupled with Gauss's law. In addition, the Onsager principle delivers the time evolution of crack length via the Griffith [38] condition

$$\gamma_{\mathrm{SE}} = -\left.\frac{\partial U_{\mathrm{elas}}}{\partial a}\right|_{u_2 \in \mathcal{S}_\Gamma}, \tag{9}$$

where

$$U_{\mathrm{elas}} = \frac{1}{2}\int_{\mathcal{V}_{\mathrm{SE}}} \varepsilon_{ij}\mathbb{C}_{ijkl}\varepsilon_{kl}\,d\mathcal{V}, \tag{10}$$

is the elastic strain energy within the electrolyte. Details of the derivations are given in Supplementary section S1.3 with material parameters for the LLZO electrolyte listed in Table 1. This highly coupled electro-mechanical formulation not only predicts the critical current density i_{CCD} but also the kinetics of crack and Li filament growth, including the shapes of the crack and Li filament, for operation of the cell at a current density $> i_{\mathrm{CCD}}$. Details of the numerical scheme to solve these coupled equations are provided in Supplementary section S2.

2.1 The critical current density

The above equations considerably simplify for the case of a non-propagating crack and can then be used to deduce the critical current density i_{CCD}. At an imposed cell current density magnitude $i_\infty \leq i_{\mathrm{CCD}}$, the pre-existing crack fills with Li and a steady-state is attained where Li^+ flux across the crack flanks is switched-off, i.e., from (6) $\sigma_n = -F\rho_{\mathrm{m}}\hat{\varphi}$. As the pre-existing

crack is assumed to contain lithium along its entire length, there can be no lithium flux into its tip until the crack is forced to propagate. Moreover, with no Li flux into the crack the solution of Gauss's law within the electrolyte is trivial as the Li^+ flux within the electrolyte is one-dimensional in the x_1 −direction. Thus, $\hat{\varphi}$ is given by

$$\hat{\varphi} = i_\infty \left[Z_0 + \frac{x_1}{\kappa} \right], \tag{11}$$

where $i_\infty = \Phi_P/(2Z_0 + (L/\kappa))$ is the magnitude of the cell current density (i.e., the current per unit electrode/electrolyte interface area) and L is the thickness of the electrolyte. The calculation of i_{CCD} then simplifies considerably for the case of an initial crack of length a_0 that emanates perpendicular from the plating electrode/electrolyte interface. From (6) and (11) it follows that the crack opening traction varies as

$$T_n = -\sigma_n = T_0 + \frac{T_0 x_1}{\kappa Z_0}, \tag{12}$$

where $T_0 = F\rho_m i_\infty Z_0$. Given this traction distribution along the crack flanks, for the practical case of $a_0/L \to 0$, there exists a closed-form solution for (9) given in Tada et al. [40]. At $i_\infty = i_{CCD}$, the relation in (9) is satisfied, and therefore the crack and filament propagate, when

$$T_0\sqrt{\pi a_0}\left[1.122 + \frac{0.683 a_0}{\kappa Z_0}\right] = \sqrt{\frac{4G\gamma_{SE/Li}}{(1-\nu)}}, \tag{13}$$

where $\gamma_{SE/Li} = \gamma_{SE} - \gamma_{adh}$ is the surface energy of an electrolyte/Li interface. Re-arranging (13) a closed-form expression for i_{CCD} follows as

$$i_{CCD} = \frac{1}{F\rho_m}\sqrt{\frac{4G\gamma_{SE/Li}}{(1-\nu)\pi a_0}}\left[1.122 Z_0 + \frac{0.683 a_0}{\kappa}\right]^{-1}. \tag{14}$$

Note that in (13-14) we have employed $\gamma_{SE/Li}$ rather than γ_{SE} as at incipient crack propagation at i_{CCD} we anticipate the crack and Li filament to propagate in unison since $\gamma_{SE/Li} < \gamma_{SE}$ ($\gamma_{adh} > 0$; see Table 1). The predicted variation (14) of i_{CCD} with electrode/electrolyte interface resistance Z_0 is included in Fig. 2c for selected choices of the initial crack length a_0 and using material parameters representative of the LLZO electrolyte as listed in Table 1. In line with numerous observations, the model predicts a reduction in i_{CCD} with increasing Z_0 and of course with increasing initial crack length a_0. The reduction in i_{CCD} with increasing Z_0 follows from the fact that a higher Z_0 induces higher crack opening tractions T_n due to a higher electric potential within the electrolyte relative to the plating electrode; see Eq. (12). With the model capturing the known dependencies of i_{CCD} on material parameters, we proceed to use the full kinetic formulation to investigate the mechanisms of crack growth and the associated shape of the crack.

Table 1: Summary of material parameters for the LLZO electrolyte.

Material parameter	Symbol	Value	Ref.
Conductivity of LLZO	κ	0.46 mS cm^{-1}	[9]
Shear modulus of LLZO	G	60 GPa	[39]
Poisson's ratio of LLZO	ν	0.2	[39]
Surface adhesion energy between LLZO/Li	γ_{adh}	0.22 J m^{-2}	[11]
Surface energy of LLZO	γ_{SE}	0.84 J m^{-2}	[11]

3. Growth of cracks in LLZO

Cracks grow in LLZO such that they are sparsely filled with Li [31] but given the very small shorting times of the cells [10] it is reasonable to assume that the cell shorts soon after the crack fully penetrates the entire thickness of the electrolyte. Thus, the Li filament and crack extend in unison in LLZO with $\dot{\zeta} \approx \dot{a}$. In our formulation this is achieved by setting $R_{\text{Tip}} = 0$ and we shall investigate the effect of $R_{\text{Tip}} > 0$ in Section 4. The justification for the choice $R_{\text{Tip}} = 0$ in LLZO is based on the fact that Density Functional Theory (DFT) calculations [41] show that LLZO surfaces have a much smaller band gap compared to the bulk and thus trap a significant number of excess electrons. This implies that as Li^+ is deposited near the tip of the filament (Fig. 2b), it easily acquires electrons, resulting in negligible resistance to the plating of Li metal at the filament tip. All calculations in this and subsequent sections are reported for an electrolyte of size $L \times W = 1\text{ mm} \times 3\text{ mm}$ which is representative of the electrolyte used in many reported experiments [29-31]. In engineering ceramics flaws/cracks on the order of grain size commonly exist. Given that the grain sizes of LLZO sintered at temperatures in the range $1100\ ^{\circ}\text{C} - 1200\ ^{\circ}\text{C}$ are typically in the range $15\ -\ 30\ \mu\text{m}$ [42], in the calculations we assume an initial flaw of length $a_0 = 25\ \mu\text{m}$ that emanates normally from the plating Li electrode/electrolyte interface and initially only contains an infinitesimally thin layer of Li. The electrode/electrolyte resistance is taken to be $Z_0 = 5\ \Omega\text{cm}^2$ [9] and in the absence of direct measurements we assume that the crack flank/Li filament resistance $Z_f = Z_0$. The calculations have been conducted by imposing a potential difference Φ_{P} across the electrodes and we report the results in terms of the imposed cell current density magnitude $i_\infty = \Phi_{\text{P}}/(L/\kappa + 2Z_0)$ which is the current in the absence of the growth of the Li filament: the large width W of the electrolyte employed in the calculations implies that the growth of the Li filament has a negligible effect upon the average cell current i_∞.

3.1 The effect of mismatch between elastic crack opening and Li flux into the crack

For cracks of initial length $a_0 = 25\ \mu\text{m}$, the critical current density $i_{\text{CCD}} = 0.71\ \text{mAcm}^{-2}$ according to Eq. (14). Now consider the case of an imposed current density of $i_\infty = 1\ \text{mAcm}^{-2} > i_{\text{CCD}}$ such that the crack and accompanying Li filament both extend. Predictions of the length of the crack and Li filament at three selected times t are shown in Fig. 3. In Fig. 3a we include distributions of normalised current density $\hat{\jmath} \equiv \sqrt{j_i j_i}/i_\infty$ while the corresponding distributions of the σ_{22} stress component are shown in Fig. 3b (also see Supplementary Video S1). First consider Fig. 3a which includes a quiver plot to show the direction of the Li^+ flux within the electrolyte and the shape of the crack (the opening of the crack has been magnified by two orders of magnitude so that the shape/profile is visible). Note that the Li filament fills the crack, as depicted by shading the crack black. The crack profiles in Figs. 3a and 3b indicate that the crack opening is maximum near the mid-length of the crack. (In contrast, the maximum opening along the length of an internally pressurised crack is typically at the crack mouth.) Throughout its loading history, the crack opening rate is positive over the entire length of the crack: i.e., the crack continues to thicken monotonically (i.e., open) consistent with observations in [30]. Thus, the bulged shape of the crack opening profile necessarily arises from the spatial variation of the Li^+ flux into the crack.

The spatio-temporal distributions of $\hat{\jmath}$ included in Fig. 3a show that far ahead of the crack tip the current density is spatially uniform and one-dimensional (1D) within the electrolyte with $\hat{\jmath} = 1$. Nearer the crack, the Li^+ flux across the crack flanks implies that the flux field is no longer one-dimensional with the current density achieving a maximum around the crack tip. While the flux magnitude decreases towards the plating electrode/electrolyte interface it is difficult to infer directly the current density j_f into the crack from these distributions of $\hat{\jmath}$.

Predictions of the normalised crack flank current density j_f/i_∞ are shown in Fig. 3c at three selected times and clearly show that the crack flank flux is a maximum at the tip and monotonically decreases towards the crack mouth at the plating electrode interface. Qualitatively we would expect such a dependence as the overpotential $\hat{\varphi}$ in (6) is expected to decrease with decreasing x_1; see for example the dependence (11) of $\hat{\varphi}$ on x_1 in the absence of flux into the growing Li filament. Now recall from (8) that the crack opening depends upon both the current density j_f and the time interval over which the crack faces exist. The bulged opening arises from the fact that while j_f decreases towards the plating electrode interface (and thereby tends to decrease δ_{Li}), τ also decreases with $\tau = 0$ for $x_1 \leq a_0$ and this tends to increase δ_{Li}.

The σ_{22} stress distributions included in Fig. 3b clearly show the high stresses associated with the crack tip stress intensity factor. More intriguing is the change in sign of σ_{22} along the crack flank. Recall that σ_{22} is related to the tractions on the crack flank by $T_n = -\sigma_{ij} n_j n_i$ where n_i is the unit normal to the crack flank pointing into the crack. Note that the definition of T_n means that its positive sense is in the direction of the inward normal to the electrolyte. It follows that $T_n = -\sigma_{22}|_{x_2=0,\ x_1 \leq a}$ where a is the current length of the crack and a negative T_n implies that the crack flank tractions are attempting to close rather than open the crack. These crack flank tractions are plotted in Fig. 3d for the three times t shown in Fig. 3b. Early in the loading history when the crack has propagated to $a = 50$ μm the tractions remain positive indicating that the Li that fluxes into the crack is tending to open the crack over its entire length. With increasing time (and crack length a) while the qualitative form of the T_n distribution remains similar important quantitative differences emerge. The traction T_n becomes negative near the crack mouth and tip indicating that the Li within the crack is attempting to close the crack at these locations. In this analysis we have assumed that the crack opening is set by (8) and thus equal to the time-integrated total Li^+ flux at any location along the crack. The calculations show that with the crack opening set by the time integrated Li^+ flux, elasticity of the electrolyte then requires the Li within the crack to close rather then open the crack at some locations and here the crack flank tractions become negative. This is most clearly seen in terms of the crack profile where the crack opening is lower near the crack mouth compared to that at midlength of the crack – this lower crack mouth opening is a direct consequence of the negative T_n near the crack mouth.

Note that the spatial gradients in Li^+ flux along the length of a crack exist for dendrites in liquid electrolytes. However, negative dendrite flank tractions do not develop in liquid electrolytes as liquids deforms with a vanishing deviatoric stress. Thus, dendrites in liquid electrolytes can take mushroom-like shapes with them bulging away from the plating electrode interface [43] but yet maintain compressive Li stresses (positive pressure) within the dendrite.

3.2 Debonding of crack flank/Li filament

The finite shear modulus of a solid electrolyte implies that the negative crack flank tractions shown above are commonplace if we assume that the crack opening is set by the Li^+ flux into the crack at every location along its flank. These negative tractions are on the order of at-least 25 MPa (Fig. 3d) and the interface between the electrolyte and the Li filament needs to sustain a tensile traction of this order if this crack/Li filament propagation mode is to exist. The adhesive strength between Li and LLZO is on the order of a few kPa [44] and thus a better approximation is that the Li/electrolyte interface along the crack flank can only sustain compressive tractions. We therefore modify the formulation summarised in Section 2 to include the constraint that $T_n(x_1) \geq 0$. Specifically, we modify the boundary conditions for the stress

equilibrium equation $\sigma_{ij,j} = 0$ over $\mathcal{S}_\Gamma$ to be a contact type boundary condition, viz., over $\mathcal{S}_\Gamma$ the crack opening $\delta(x_1) = \delta_{\mathrm{Li}}(x_1)$ where δ_{Li} is given by (8) if $T_n(x_1) \geq 0$; otherwise, $T_n(x_1) = 0$ and the crack opening $\delta(x_1) > \delta_{\mathrm{Li}}(x_1)$ is an outcome of the solution of the elasticity problem; see Supplementary section S3 for further details.

The temporal evolution of the debonding of the Li filament from the electrolyte is a complex phenomenon that ultimately results in a complicated structure of a partially filled crack as observed via X-ray CT for LLZO [31]. To illustrate this, we consider the case analysed in Section 3.1 and first illustrate the process by which the Li filament detaches from the electrolyte that results in partial filling of the crack near the crack mouth. The shape of the crack near its mouth is shown in Fig. 4a at three selected times, with the crack lengths also indicated. At $t = 155$ s, the crack is fully filled with Li over the region shown but the corresponding spatial distribution of T_n shown in Fig. 4b suggests that the crack flanks are about to debond from the Li filament at the mouth ($x_1 = 0$) as $T_n(x_1 = 0) = 0$. When debonding occurs we assume that an atomistically thin layer of Li is left adhered to the electrolyte flanks so that further Li^+ flux into the crack can continue with the fluxing Li^+ acquiring an electron from this layer that is connected to the plating electrode. This continued flux gives a Li deposition rate $\dot{\delta}_{\mathrm{Li}} < \dot{\delta}$ with the traction being maintained at $T_n = 0$ at $x_1 = 0$. In fact, with increasing time the debonding progresses towards the crack tip (i.e., $x_1 > 0$) and the expected Li filament structure within the crack and the corresponding traction distribution are plotted in Fig. 4 at $t = 180$ s. At this instant, $T_n = 0$ for $x_1 < 20$ μm and this portion of the crack is partially filled with Li. In Fig. 4a we have shaded the crack volume to show three separate regions: (i) Li deposited before detachment is shaded grey; (ii) Li deposited after detachment is shaded pink and (iii) a void or empty region is shaded blue. We emphasize that we have assumed that the Li within the crack is rigid. This implies that we are unable to predict the precise Li filament morphology within the partially filled crack. The Li morphology shown in Fig. 4a assumes that the Li does not deform and thus the voided region is shown in Fig. 4a between the Li that was initially deposited (grey in Fig. 4a) and the Li that is deposited after detachment occurred (shaded pink in Fig. 4a). Nevertheless, it is clear from Fig. 4a that the extent of the empty region is largest at $x_1 = 0$ (see structure at time $t = 220$ s). This is a direct consequence of the fact that detachment first occurred at $x_1 = 0$ and that the crack opening rates are the largest at the crack mouth.

The geometry of the Li filament within the partially filled crack shown in Fig. 4a is inaccurate due to the assumption that the Li is rigid. However, our aim here is not to describe the Li filament geometry in detail but rather quantify the level of filling of the crack and its effect on crack propagation. Keeping this in mind, we define a filling ratio c of the crack with its rate of change given by

$$\dot{c}(x_1) = -\frac{1}{\delta(x_1)}\left\{\dot{\delta}(x_1) - \dot{\delta}_{\mathrm{Li}}(x_1)\right\}, \tag{15}$$

where $\{\cdot\}$ denotes the Macaulay brackets and (15) is integrated at locations x_1 along $\mathcal{S}_\Gamma$ with initial conditions $c(x_1) = 1$. Then the crack flank tractions $T_n(x_1) \geq 0$ where $c(x_1) = 1$ and $T_n = 0$ where $c(x_1) < 1$. This coarse graining, whereby we only calculate the difference between the crack opening and deposition of Li, not only has the advantage of numerical convenience but also makes no assumptions about the geometry of the Li filament within the partially filled crack. Predictions using this approach are included in Fig. 5 (for the case analysed for Fig. 3) with flux distributions shown in Fig. 5a and the corresponding stresses σ_{22} in Fig. 5b (also see Supplementary Video S2). Two key differences are apparent: (i) in line with typical crack opening profiles, the opening increases monotonically behind the crack tip

with the maximum opening at the mouth ($x_1 = 0$) and (ii) the stresss σ_{22} do not change sign along the crack flanks. This is further clarified via the T_n distributions shown in Fig. 5c where we see that the tractions vanish near the mouth and tip of the crack, i.e., at locations where $T_n < 0$ in Fig. 3d. At these locations where $T_n = 0$, the crack is partially filled with Li as seen in Fig. 5d where we show the spatial distribution of the crack filling ratio c for two selected crack lengths a.

The predictions that cracks in LLZO are partially filled with Li are consistent with recent X-ray CT observations [31] (see also Fig. 1b) and our model gives a physical understanding of the phenomenon. When debonding of the Li filament from the electrolyte is permitted not only do partially filled cracks develop but negative tractions that tend to close the crack do not develop. These negative tractions tend to reduce the tip stresses (and stress intensity factor) and the absence of these negative tractions is expected to enhance crack growth rates. Predictions of the temporal evolution of the crack length a with time are included in Fig. 6a for 3 imposed current densities i_∞ for the two sets of simulations, viz. (i) no debonding and (ii) debonding permitted between the Li and the electrolyte along the crack flank. Clearly, when debonding is prevented, the growth of the crack slows down due to crack closing tractions (negative T_n) being imposed on the crack flanks near the tip and mouth of the crack. Predictions assuming no debonding and with debonding permitted of the average crack velocity $\langle \dot{a} \rangle$ (over the interval $150\ \mu\text{m} \leq a \leq 250\ \mu\text{m}$) as a function of i_∞ are included in Fig. 6b along with corresponding measurements from Kazyak et al. [10]. The predictions assuming full adhesion and no debonding underestimate the crack velocity while predictions that allow debonding with the crack flank tractions constrained to $T_n \geq 0$ agree remarkably well with the measurements. Thus, the predictions of partially filled cracks are not only consistent with direct tomographic observations of the Li filament structure within cracks but are also consistent with more macroscopic measurements of the growth rate of cracks.

4. Growth of dry cracks

Ning et al. [29] and Hao et al. [30] have used a combination of in-situ X-ray CT (see also Fig. 1a) and spatially mapped X-ray diffraction to demonstrate that the crack tip in sulphide electrolytes outruns the Li filament such that cracks traverse the entire electrolyte with Li absent from the crack over a finite length behind the crack tip. Thus, cracking of the electrolyte can occur before the cell short-circuits. In our model we attribute the difference in behaviour of LLZO and sulphide electrolytes to a difference in the magnitude of the Li filament tip resistance R_{Tip}. DFT calculations [41] have shown that the surface band gap for sulphide electrolytes is large compared to the bulk and therefore we do not anticipate an accumulation of excess electrons on the surface of the fractured LPS. Consequently, we anticipate that a substantial resistance exists for Li^+ to acquire electrons near the Li filament tip (see Fig. 2b) and expect that, unlike LLZO, $R_{\text{Tip}} \gg 0$ for sulphide electrolytes. While direct measurements of R_{Tip} have not been reported in the literature we summarise the results of calculations here to show the effect of $R_{\text{Tip}} > 0$ on the growth of the crack and Li filament. The aim is to show the effect of R_{Tip} upon the mechanism of crack and Li filament propagation, and thus it suffices to keep all parameters fixed at the values for LLZO (Table 1) and only change R_{Tip} for the calculations reported in this section.

Predictions of the growth of the crack/Li filament initiating from an initial crack of length $a_0 = 25\ \mu\text{m}$ are included in Fig. 7 (also see Supplementary Video S3). with the choice of $R_{\text{Tip}} = 22\ \Omega\text{cm}$ (all loading parameters are the same as for the cases in Fig. 3 and 5 and we restrict

attention to the case when debonding is permitted such that $T_n \geq 0$). The high value of R_{Tip} results in two major differences from the corresponding $R_{\text{Tip}} = 0$ results in Fig. 5:

(i) The Li filament and crack propagate simultaneously until $t \approx 90\text{s}$ ($a = \zeta \approx 50$ μm) but subsequently the crack tip accelerates ahead of the Li filament with the near crack tip region being devoid of Li. This is consistent with observations reported in [30]; see their Fig. 3e. Thus, while the stress concentration persists near the crack tip, the flux concentration is no longer at the crack tip but further back and located at the Li filament tip. This is in contrast to the $R_{\text{Tip}} = 0$ case.

(ii) The crack propagation rate is lower compared to the $R_{\text{Tip}} = 0$ case. The crack propagates to $a = 500$ μm in 250 s and 315 s for $R_{\text{Tip}} = 0$ and $R_{\text{Tip}} = 22$ Ωcm, respectively.

To understand the lower crack propagation rate, note that shorter Li filaments imply that the crack opening tractions are now exerted over a smaller fraction of the crack flank (compare Fig. 7c with Fig. 5c). Thus, the magnitudes of the tractions need to be higher to allow the crack to propagate and these higher tractions requires greater crack openings, i.e. thicker Li filaments. To show this we compare the crack opening profiles for the $R_{\text{Tip}} = 0$ case from Fig. 5 and the $R_{\text{Tip}} = 22$ Ωcm case in Fig. 7d. Until $a \approx 50$μm the crack and Li filament propagate in unison and the crack profiles are similar in both cases, but for $a > 50$μm the crack openings are larger for $R_{\text{Tip}} = 22$ Ωcm compared to those for $R_{\text{Tip}} = 0$. These larger openings induce larger crack flanks tractions (compared Figs. 5c and 7c). The larger required crack opening take longer to be built-up by the Li^+ fluxes, and this reduces the crack propagation rate.

4.1 Effect of the filament tip resistance

Predictions of the temporal evolution of the crack length a and Li filament length ζ are included in Fig. 8a for three values of the filament tip resistance R_{Tip} and an imposed current density $i_\infty = 1$ mAcm^{-2}. As discussed above, the crack and Li filament propagate in unison for $R_{\text{Tip}} = 0$. However, for the higher values of R_{Tip} not only does the crack tip propagate more slowly but the divergence between the temporal evolution of a and of ζ also increases with increasing R_{Tip}. An immediate consequence is that the time to crack the electrolyte and the time at which the cell shorts will differ at the higher values of R_{Tip}. This is clearly observed in [29,30] where X-ray imaging shows that the electrolyte has cracked but the cell has not shorted at the time of complete fracture of the electrolyte.

To quantify this difference, we define two failure times: (i) t_{crack} for the cracking of the electrolyte, i.e., the time when $a = L$ and (ii) the shorting time t_{short} when $\zeta = L$. Note that for time $t > t_{\text{crack}}$ the electrolyte has fractured with tractions $T_n = 0$ on the crack flanks and the solution of the subsequent filament growth problem is a pure electrochemical solution with no mechanical coupling. Predictions of t_{crack} and t_{short} are included in Fig. 8b as a function of the imposed current density i_∞ for $R_{\text{Tip}} = 0$ and $R_{\text{Tip}} = 22$ Ωcm. For $R_{\text{Tip}} = 0$, $t_{\text{crack}} = t_{\text{short}}$ so that cracking of the electrolyte is synonymous with shorting of the cell in line with observations for LLZO. On the other hand, shorting occurs significantly after cracking of the electrolyte in the $R_{\text{Tip}} = 22$ Ωcm case and this is qualitatively consistent with observations for sulphide electrolytes. In all cases, the cracking and shorting times decrease with increasing i_∞ as the flux of Li into the crack increases as i_∞ increases.

5. Concluding remarks

A variational principle for modelling the ingress of Li into solid electrolytes has been developed by making use of Onsager formalism. The Onsager principle [36-37] allows us to couple together the elastic deformation and cracking of the electrolyte, the electrochemical driving forces in the cell and the ion transport dissipative processes in the electrolyte bulk and across the electrolyte/electrode and electrolyte/crack interfaces. The kinetics of crack/Li filament propagation along with the shapes of the crack and Li filament are natural outcomes of the solution to the variational problem.

Unlike liquid electrolytes, in solid electrolytes the elasticity of the solid implies that the crack cannot assume arbitrary shapes if the tractions along the Li filament/crack interface are to remain compressive. Consequently, the mismatch between the time-integrated flux of Li^+ ions into the crack and elastic opening of the crack can result in sparse filling of the cracks with Li, while the resistance to the ability of Li^+ ions to acquire electrons at the Li filament tip implies that the crack can propagate ahead of the Li filament in some cases. The predictions are not only in good qualitative agreement with X-ray CT observations of the cracking of LLZO and LPS electrolytes but are also in excellent quantitative agreement with measured crack velocities.

The framework provides a comprehensive understanding of the kinetics of cracking and Li filament propagation in solid electrolytes. It shows that the mismatch between the elastic crack opening and the flux of Li^+ ions into the cracks is a maximum near the mouth of the crack at the interface with the plating electrode. Direct X-ray CT observations to measure the extent of filling of cracks as a function of position within the electrolyte have not been reported to-date. Such observations are desirable and will serve to further test the fidelity of the modelling framework introduced here.

Acknowledgements

The authors are grateful for helpful discussions with Profs. Peter Bruce and Clare Grey. NAF, PRS and SH acknowledge support by the Faraday Institution [Solbat, grant number FIRG007]. PRS acknowledges the support of The Royal Academy of Engineering (CiET1718/59).

References

[1] N. Kamaya, K. Homma, Y. Yamakawa, M. Hirayama, R. Kanno, M. Yonemura, T. Kamiyama, Y. Kato, S. Hema, K. Kawamoto, A. Mitsui, *Nat. Mater.*, **2011**, 10(9), 682-686.

[2] P. G. Bruce, S. A. Freunberger, L. J. Hardwick, J-M Tarascon, *Nat. Mater.*, **2012**, 11(1), 19-29.

[3] K. Takada, *Acta Mater.*, **2013**, 61(3), 759-770.

[4] K. B. Hatzell, X. Chelsea Chen, C. L. Cobb, N. P. Dasgupta, M. B. Dixit, L. E. Marbella, M. T. McDowell, P.P. Mukherjee, A. Verma, V. Viswanathan, A. S. Westover, *ACS Energy Lett.*, **2020**, 5(3), 922-934.

[5] L. Porz, T. Swamy, B. W. Sheldon, D. Rettenwander, T. Frömling, H. L. Thaman, S. Berendts, R. Uecker, W. C. Carter, Y-M. Chiang, *Adv. Energy Mater.*, **2017**, 7(20), 1701003.

[6] F. Flatscher, M. Philipp, S. Ganschow, H. M. R. Wilkening, D. Rettenwander, *J. Mater. Chem. A,* **2020**, 8(31), 15782-15788.

[7] L. Cheng, W. Chen, M. Kunz, K. Persson, N. Tamura, G. Chen, M. Doeff, *ACS Appl. Mater. Interfaces*, **2015**, *7*(3), 2073-2081.
[8] A. Sharafi, H. M. Meyer, J. Nanda, J. Wolfenstine, J. Sakamoto, *J. Power Sources*, **2016**, 302, 135-139.
[9] A. Sharafi, C. G. Haslam, R. D. Kerns, J. Wolfenstine, J. Sakamoto, *J. Mater. Chem. A*, **2017**, 5(40) 21491-21504.
[10] E. Kazyak, R. Garcia-Mendez, W. S. LePage, A. Sharafi, A. L. Davis, A. J. Sanchez, K-H. Chen, C. Haslam, J. Sakamoto, N. P. Dasgupta, *Matter*, **2020**, 2(4) 1025-1048.
[11] A. Sharafi, E. Kazyak, A. L. Davis, S. Yu, T. Thompson, D. J. Siegel, N. P. Dasgupta, J. Sakamoto, *Chem. Mater.*, **2017**, 29(18) 7961-7968.
[12] C-L. Tsai, V. Roddatis, C. Vinod Chandran, Q. Ma, S. Uhlenbruck, M. Bram, P. Heitjans, O. Guillon. *ACS Appl. Mater. Interfaces*, **2016**, 8(16) 10617-10626.
[13] J. Kasemchainan, S. Zekoll, D. Spencer Jolly, Z. Ning, G. O. Hartley, J. Marrow, P. G. Bruce, *Nat. Mater.*, **2019**, 18(10) 1105-1111.
[14] T. Deng, X. Ji, Y. Zhao, L. Cao, S. Li, S. Hwang, C. Luo, P. Wang, H. Jia, X. Fan, X. Lu, *Adv. Mater.*, **2020**, 32(23) 2000030.
[15] M.B. Dixit, M. Regala, F. Shen, X. Xiao, K. B. Hatzell, *ACS Appl. Mater. Interfaces*, **2018**, 11(2), 2022-2030.
[16] K. J. Harry, D. T. Hallinan, D. Y. Parkinson, A. A. MacDowell, N. P. Balsara, *Nat. Mater.*, **2014** 13(1), 69-73.
[17] D. Spencer Jolly, Z. Ning, J. E. Darnbrough, J. Kasemchainan, G. O. Hartley, P. Adamson, D. E. J. Armstrong, J. Marrow, P. G. Bruce, *ACS Appl. Mater. Interfaces*, **2019**, 12(1), 678-685.
[18] L. Barroso-Luque, Q. Tu, G. Ceder, *J. Electrochem. Soc.*, **2020**, 167(2), 020534.
[19] P. Barai, A.T. Ngo, B. Narayanan, K. Higa, L. A. Curtiss, V. Srinivasan, *J. Electrochem. Soc.*, **2020** 167(10), 100537.
[20] P. Barai, K. Higa, V. Srinivasan, *J. Electrochem. Soc.*, **2018**, 165(11), A2654.
[21] L. Porz, T. Swamy, B. W. Sheldon, D. Rettenwander, T. Frömling, H. L. Thaman, S. Berendts, R. Uecker, W. C. Carter, Y-M. Chiang, *Adv. Energy Mater.*, **2017**, 7(20), 1701003.
[22] M. Klinsmann, F. E. Hildebrand, M. Ganser, R. M. McMeeking, *J. Power Sources*, **2019**, 442 227226.
[23] F. Yang, *Phys. Chem. Chem. Phys.*, **2020**, 22(24), 13737-13745.
[24] R. D. Armstrong, T. Dickinson, J. Turner, *Electrochim. Acta*, **1974**, 19(5) 187-192.
[25] G. Bucci, J. Christensen, *J. Power Sources*, **2019**, 441, 227186.
[26] H. Haftbaradaran, S. Esmizadeh, A. Salvadori, *Int. J. Solids Struct.*, **2022**, 254, 111852.
[27] S. S. Shishvan, N. A. Fleck, R. M. McMeeking, V. S. Deshpande, *J. Power Sources*, **2020**, 456, 227989.
[28] S. S. Shishvan, N. A. Fleck, R. M. McMeeking, V. S. Deshpande, *Acta Mater.*, **2020**, 196, 444-455.
[29] Z. Ning, D. Spencer Jolly, G. Li, R. De Meyere, S. D. Pu, Y. Chen, J. Kasemchainan, J. Ihli, C. Gong, B. Liu, D. L. R. Melvin, A. Bonnin, O. Magdysyuk, P. Adamson, G. O. Hartley, C. W. Monroe, T. J. Marrow, P. G. Bruce, *Nat. Mater.*, **2021**, 20(8), 1121-1129.
[30] S. Hao, S. R. Daemi, T. MM. Heenan, W. Du, C. Tan, M. Storm, C. Rau, D. JL. Brett P. R. Shearing, *Nano Energy*, **2021**, 82, 105744.
[31] S. Hao, J. J. Bailey, F. Iacoviello, J. Bu, P. S. Grant, D. JL. Brett, P. R. Shearing, *Adv. Funct. Mater.*, **2021**, 31(10) 2007564.
[32] C. D. Fincher, D. Ojeda, Y. Zhang, G. M. Pharr, M. Pharr, *Acta Mater.*, **2020**, 186, 215-222.

[33] C. Xu, Z. Ahmad, A. Aryanfar, V. Viswanathan, J. R. Greer, *Proc. Natl. Acad. Sci. U.S.A*, **2017**, 114(1) 57-61.
[34] L. Zhang, T. Yang, C. Du, Q. Liu, Y. Tang, J. Zhao, B. Wang, T. Chen, Y. Sun, P. Jia, H. Li, L. Geng, J. Chen, H. Ye, Z. Wang, Y. Li, H. Sun, X. Li, Q. Dai, Y. Tang, Q. Peng, T. Shen, S. Zhang, T. Zhu, J. Huang, *Nat. Nanotechnol.,* **2020**, 15(2), 94-98.
[35] C. D. Fincher, C. E. Athanasiou, C. Gilgenbach, M. Wang, B. W. Sheldon, W. Craig Carter, Y-M. Chiang, *ChemRxiv*, **2022**.
[36] L. Onsager, *Phys. Rev.* **1931**, 37, 405-426.
[37] L. Onsager, *Phys. Rev.* **1931**, 38, 2265-2279.
[38] A. A. Griffith, *Phil. Trans. Roy. Soc. London A*, **1921**, 221(582-593), 163-198.
[39] J. E. Ni, E. D. Case, J. S. Sakamoto, E. Rangasamy, J. B. Wolfenstine, *J. Mater. Sci.*, **2012**, 47(23), 7978-7985.
[40] H. Tada, P. Paris, G. Irwin, The stress analysis of cracks handbook, New York: ASME Press, **2000**.
[41] H-K. Tian, Z. Liu, Y. Ji, L-Q. Chen, Y. Qi, *Chem. Mater.*, **2019**, 31(18), 7351-7359.
[42] A. Sharafi, C.G Haslam, R.D. Kerns, J. Wolfenstine, J. Sakamoto, *J. Mater. Chem. A*, **2017**, 5, 21491-21504.
[43] K. N. Wood, E. Kazyak, A. F. Chadwick, K-H. Chen, J-G. Zhang, K. Thornton, N. P. Dasgupta, *ACS Cent. Sci.*, **2016**, 2(11), 790-801.
[44] M. Wang, J. Sakamoto, *J. Power Sources*, **2018**, 377, 7-11.

Figures

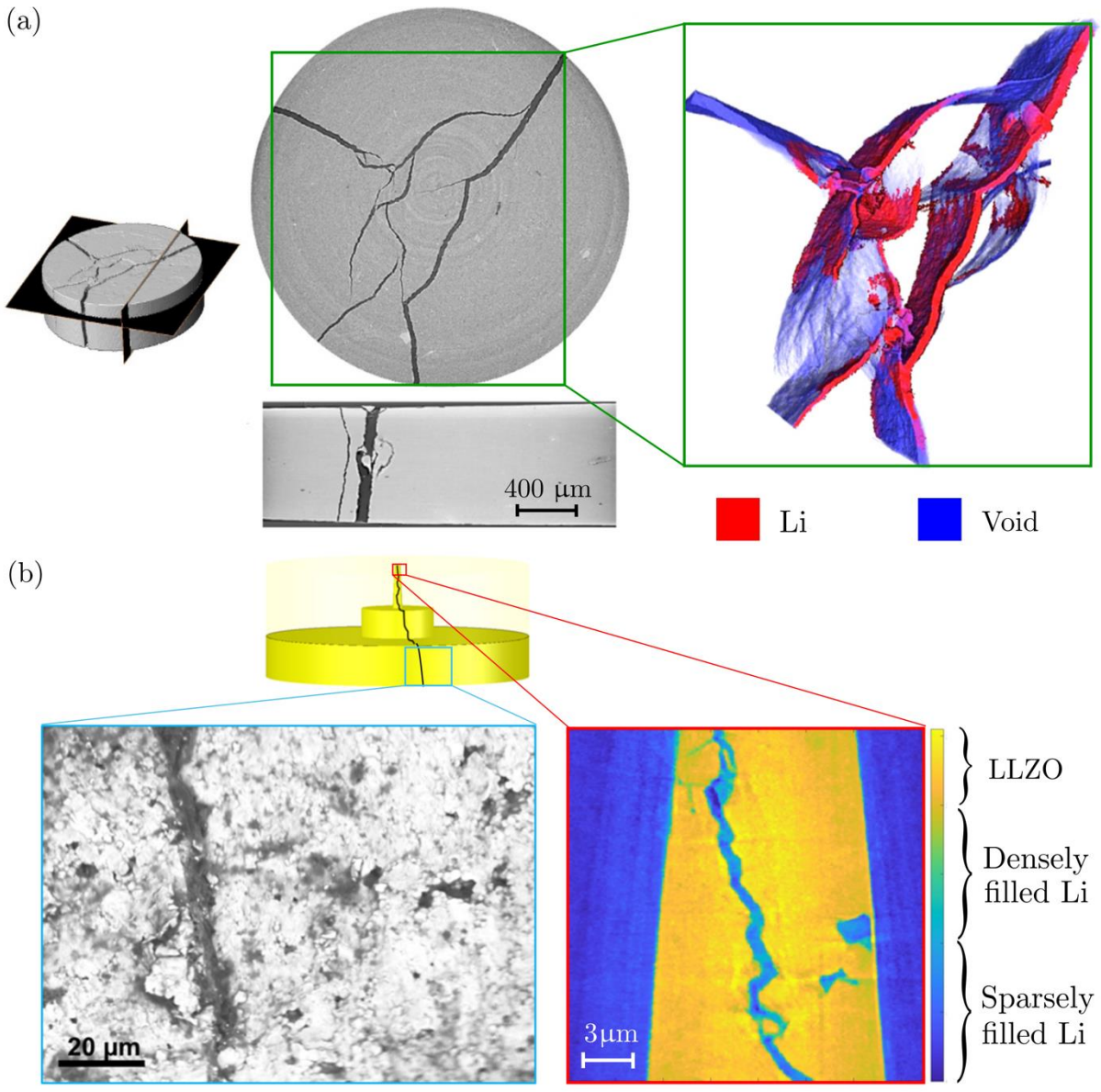

Figure 1: (a) Optical micrograph and corresponding X-ray CT reconstruction of the crack in LPS showing that while the electrolyte has completely cracked the Li is only present near the mouth of the crack at the plating electrode interface. Modified from [30] with the image on the left indicating the two planes over which the zoom-ins are shown. (b) Scanning electron microscope (SEM) image and X-ray CT reconstruction of a crack within LLZO showing that the crack is partially filled with Li. Data reconstructed from measurements taken in [31].

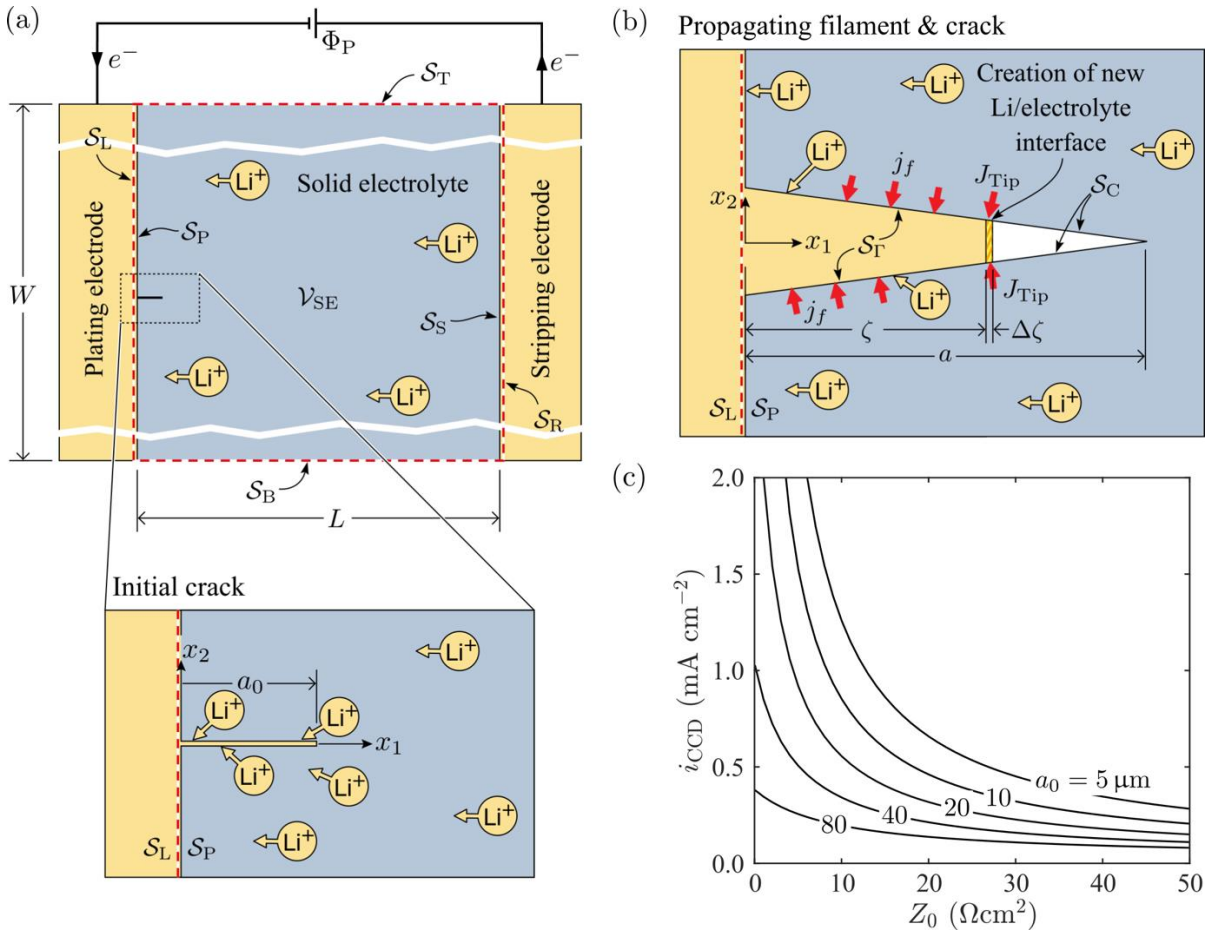

Figure 2: (a) Sketch of the symmetric cell analysed with the system of volume $\mathcal{V}$ that is bounded by $\mathcal{S} \equiv \mathcal{S}_L \cup \mathcal{S}_R \cup \mathcal{S}_T \cup \mathcal{S}_B$. The electrolyte of size $L \times W$ has a volume labelled $\mathcal{V}_{SE}$ and the plating and stripping electrode interfaces are labelled $\mathcal{S}_P$ and $\mathcal{S}_S$, respectively. There exists an initial crack of length a_0 that is perpendicular to $\mathcal{S}_P$. (b) Sketch showing the plating of the Li at the tip of the filament with a current J_{Tip} along with the current density $j_f = j_i n_i$ across the crack flanks along with crack surface $\mathcal{S}_\Gamma$ along which the Li filament of length ζ is present with the remainder of the crack of length a being dry. The dry crack flanks are labelled $\mathcal{S}_C$. (c) Predictions of the critical current density i_{CCD} as a function of electrode/electrolyte interface resistance Z_0 for selected values of a_0 using properties representative of LLZO (Table 1).

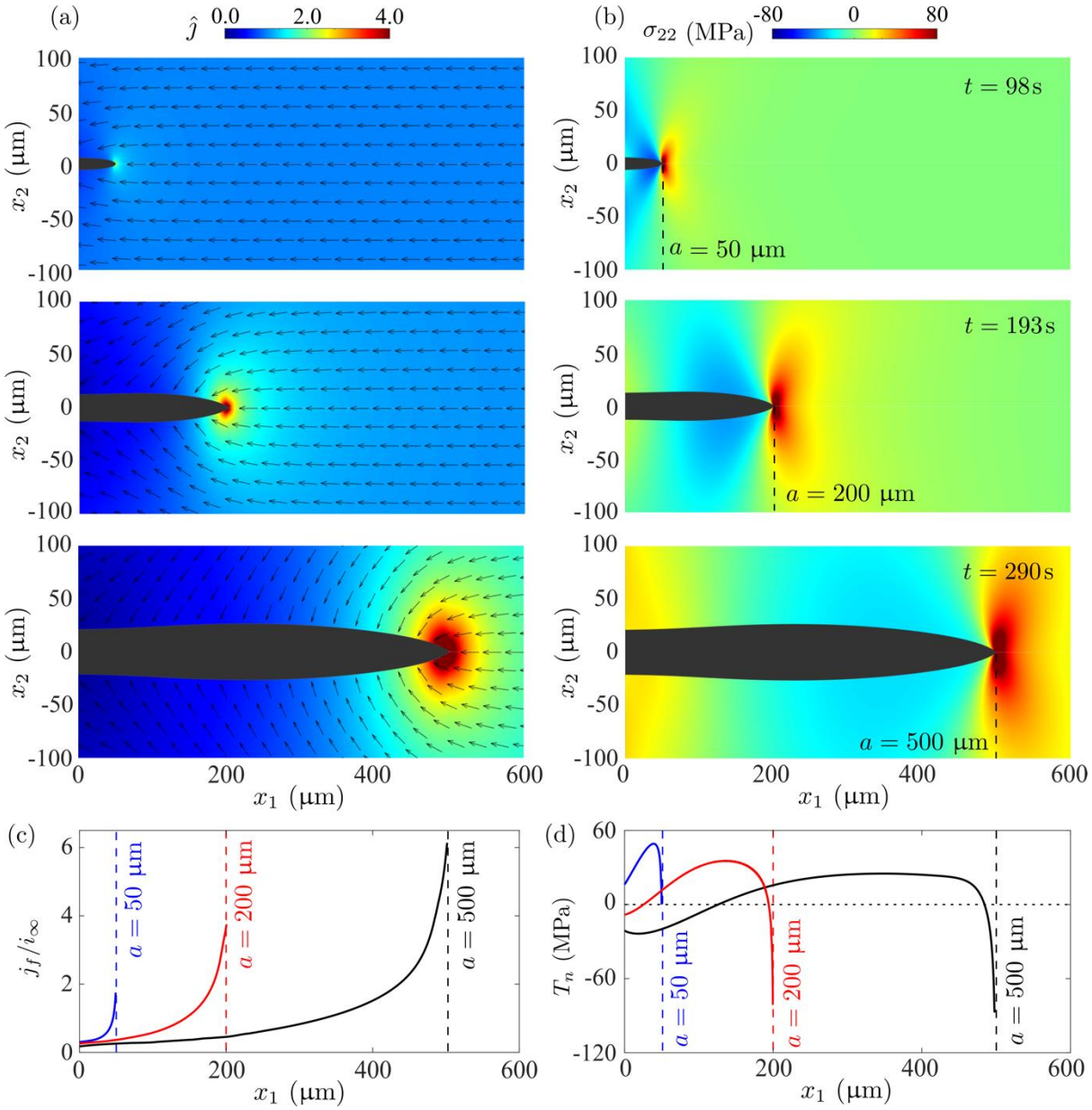

Figure 3: Predictions of the evolution of the (a) normalised current density $\hat{\jmath} \equiv \sqrt{j_i j_i}/i_\infty$ and (b) stress σ_{22} within the electrolyte for a cell with $R_{\text{Tip}} = 0$ subjected to an imposed current density $i_\infty = 1$ mAcm^{-2}. In (a) we include a quiver plot to show the direction of Li^+ flux within the electrolyte. Debonding of the Li from the crack flanks is not permitted. The opening of the crack is magnified $\times 200$ so that the crack profile is clearly visible. The time t and current crack length a are indicated for each of the three time instants (also see Supplementary Video S1). Corresponding predictions of the (c) normalised crack flank current density j_f/i_∞ and (d) crack flank tractions T_n. Note that a positive value of T_n contributes to opening the crack whereas a negative one does the opposite.

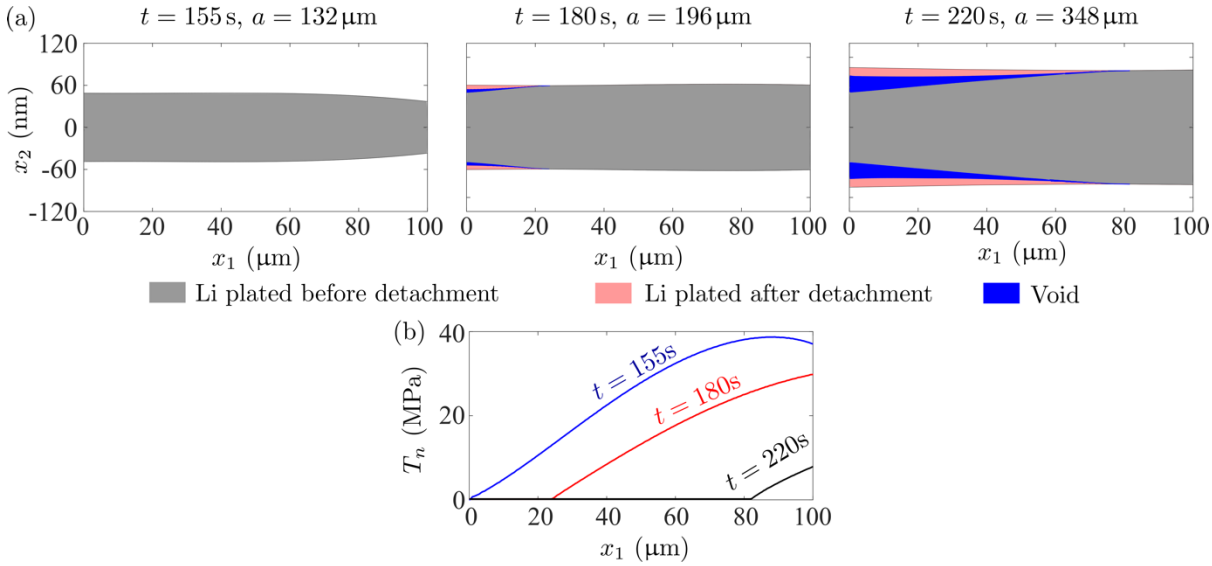

Figure 4: Structure of the Li filament within the crack near the crack mouth for the case of a cell subjected to an imposed current density $i_\infty = 1\ \mathrm{mAcm}^{-2}$ with $R_{\mathrm{Tip}} = 0$. (a) The Li within the crack at three time instants with $t = 155\ \mathrm{s}$ corresponding to the instant when debonding is about to commence at the crack mouth. Subsequently we show the Li filament geometry within the crack with the shading indicating the empty regions and Li deposited before and after detachment from the crack flanks. Note that the x_2-axis scale is in nm such that the crack opens by less than 100 nm when it has propagated to a length $a \approx 350\ \mu\mathrm{m}$. (b) The corresponding evolution of the crack flank tractions T_n that are not permitted to be negative.

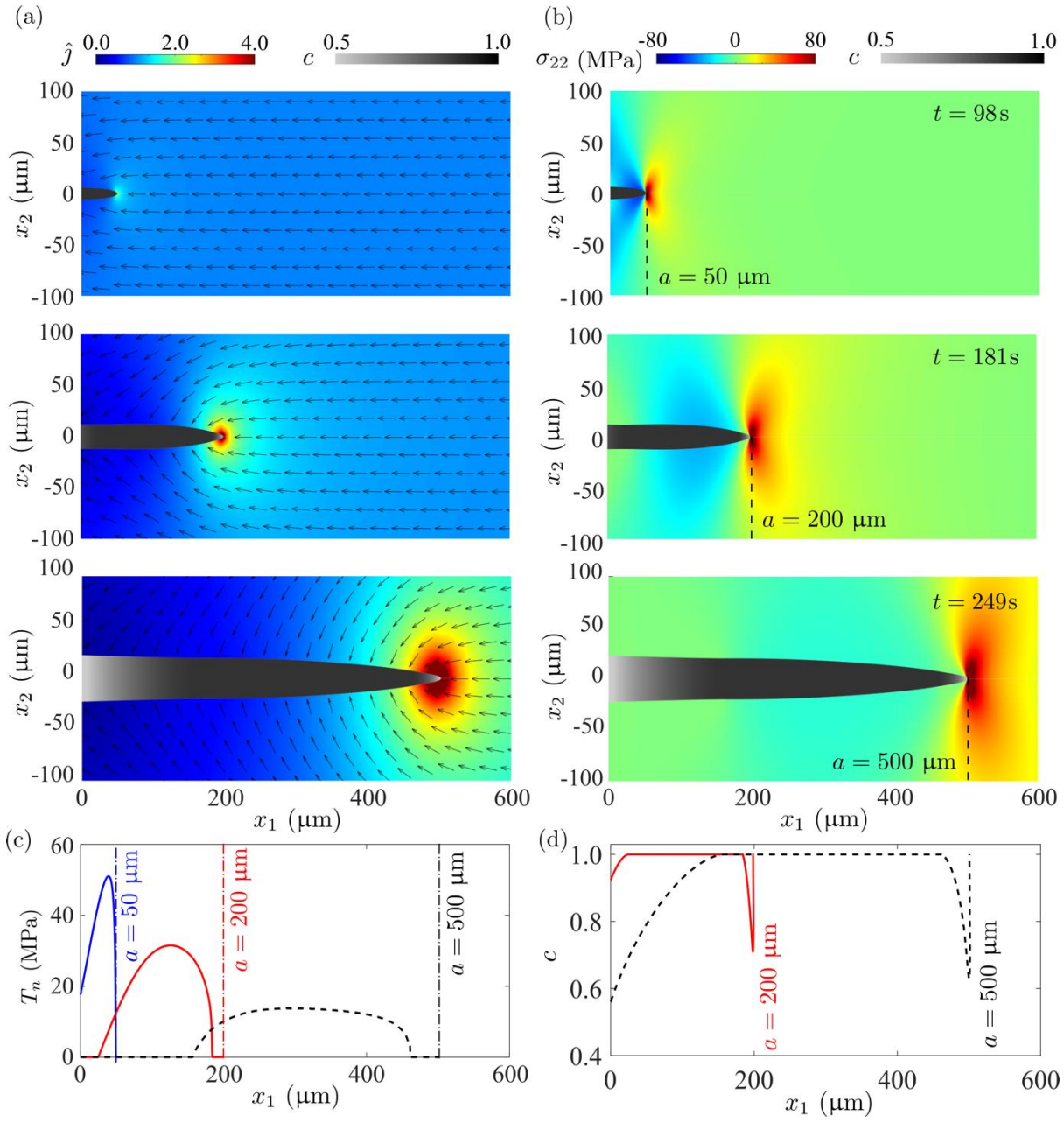

Figure 5: The effect of debonding between the Li filament and the crack flank on the predictions of the evolution of the (a) normalised current density $\hat{j} \equiv \sqrt{j_i j_i}/i_\infty$ and (b) stress σ_{22} within the electrolyte for a cell with $R_{\text{Tip}} = 0$ subject to an imposed current density $i_\infty = 1\ \text{mAcm}^{-2}$. In (a) we include a quiver plot to show the direction of the Li^+ flux within the electrolyte. Debonding between the Li filament and crack flanks is assumed to occur such that the crack flank traction $T_n \geq 0$. The opening of the crack is magnified $\times\, 200$ so that the crack profile is clearly visible. The time t and current crack length a are indicated for each of the three time instants (also see Supplementary Video S2). Corresponding predictions of the (c) crack flank traction T_n and (d) filling fraction c along the crack.

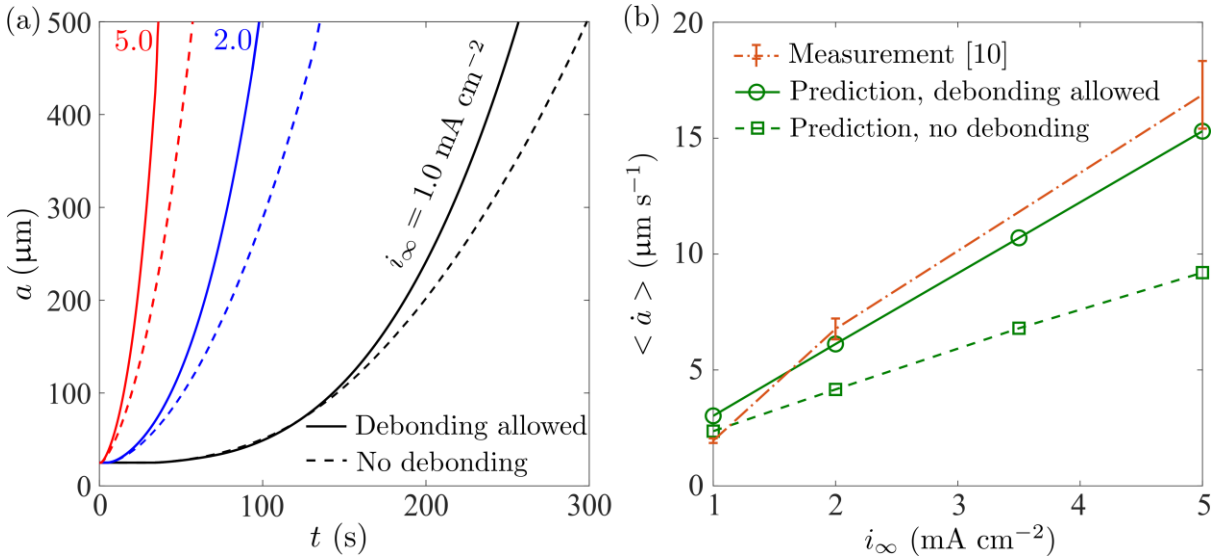

Figure 6: (a) Predictions of the temporal evolution of the crack length a with $R_{\mathrm{Tip}} = 0$ for three values of the imposed current density i_∞. Results are shown for the cases when debonding is not permitted and when debonding of the Li from the crack flanks is allowed such that $T_n \geq 0$. (b) Comparison between predictions and measurements [10] of the average crack speed $\langle \dot{a} \rangle$ over the interval $150\ \mu\mathrm{m} \leq a \leq 250\ \mu\mathrm{m}$ as a function of i_∞. The predictions for the both the debonding allowed and prevented cases are included.

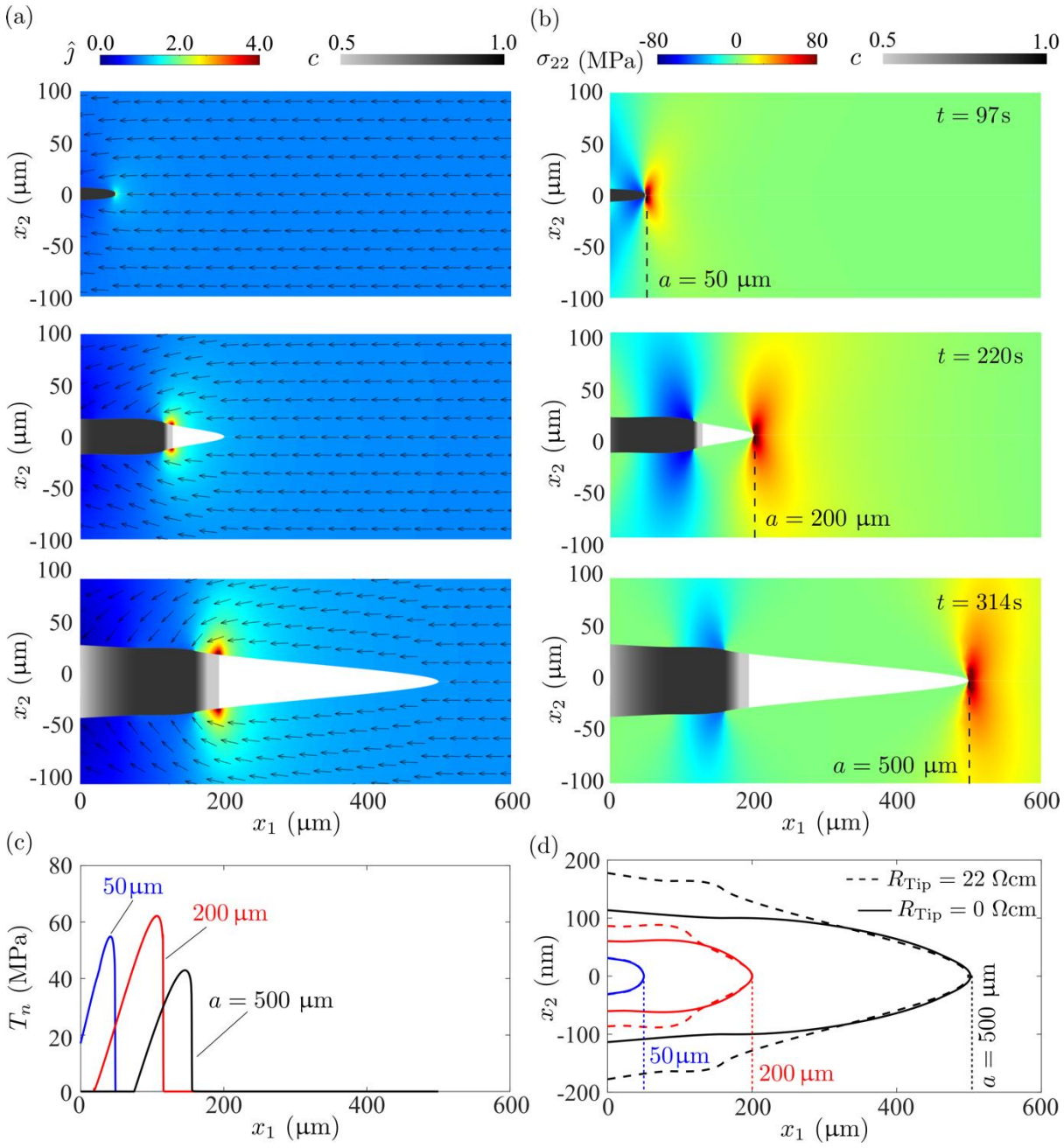

Figure 7: Predictions of the evolution of the (a) normalised current density $\hat{j} \equiv \sqrt{j_i j_i}/i_\infty$ and (b) stress σ_{22} within the electrolyte for a cell with $R_{\mathrm{Tip}} = 22$ Ωcm subjected to an imposed current density $i_\infty = 1$ mAcm^{-2}. In (a) we include a quiver plot to show the direction of the Li^+ flux within the electrolyte. Debonding is assumed to occur such that the crack flank traction $T_n \geq 0$. The opening of the crack is magnified × 200 so that the crack profile is clearly visible. The time t and current crack length a are indicated for each of the three time instants (also see Supplementary Video S3). (c) Corresponding predictions of the crack flank traction T_n and (d) comparison of the crack profile for the $R_{\mathrm{Tip}} = 22$ Ωcm case with the $R_{\mathrm{Tip}} = 0$ case of Fig. 5.

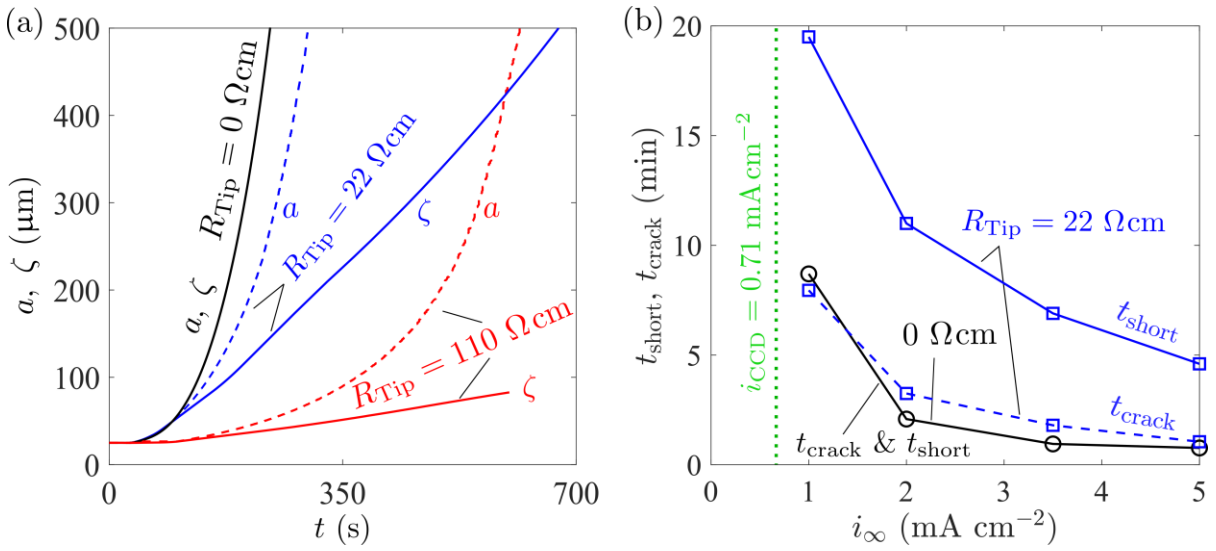

Figure 8: (a) Predictions of the temporal evolution of the crack length a and Li filament length ζ for a cell subjected to an imposed current density $i_\infty = 1\ \mathrm{mAcm^{-2}}$. Results are shown for three choices of the filament tip resistance R_{Tip}. (b) Predictions of the time t_{crack} to crack the electrolyte and the time t_{short} to short the cell as a function of i_∞ for two choices of R_{Tip}. These predictions are for an electrolyte of thickness $L = 1$ mm.

SUPPLEMENTARY MATERIAL

Ingress of Li into solid electrolytes: cracking and sparsely filled cracks

D. Mukherjee[a], S. Hao[b,c], P.R. Shearing[b,d], R.M. McMeeking[e], N.A. Fleck[a,d], and V.S. Deshpande[a,d*]

[a] *Department of Engineering, University of Cambridge, Cambridge CB2 1PZ, UK*
[b] *Electrochemical Innovation Lab, Department of Chemical Engineering, University College London, London WC1E 7JE, UK*
[c] *Institute of New Energy Material Chemistry, School of Materials Science and Engineering, Nankai University, Tianjin 300021, China*
[d] *The Faraday Institution; Quad One, Harwell Science and Innovation Campus, Didcot, UK*
[e] *Department of Mechanical Engineering & Materials Department, University of California, Santa Barbara CA 93106, USA*

Contents:

S1: A variational principle for Li dendrite and dry crack propagation in solid electrolytes
S2: Numerical solution methodology
S3: Modification of variational principle and numerical solution technique when debonding between filament and crack flanks is permitted
Supplementary References
Supplementary Figure S1
Supplementary Video S1
Supplementary Video S2
Supplementary Video S3

S1. A variational principle for Li dendrite and dry crack propagation in solid electrolytes

In this section we derive a variational principle for the propagation of a Li filament and a dry crack in solid electrolytes. Here we constrain ourselves to the case when the Li filament is perfectly bonded to the crack flanks of the electrolyte (Fig. S1) with the interface assumed to be capable of sustaining tensile tractions. This condition is relaxed in a small modification to the principle presented in Section S3.

S1.1 Free-energy of the Li filament and chemical potentials of Li within the electrolyte and the Li filament

First consider the metallic Li filament that is electrically neutral. Consider a volume Ω of Li metal comprising N_{L} moles of lattice sites that are occupied by N_{Li} moles of Li atoms such that $\Omega \equiv (N_{\mathrm{Li}}\Omega_{\mathrm{Li}} + N_{\mathrm{v}}\Omega_{\mathrm{v}})$ where Ω_{Li} is the molar volume of Li and Ω_{v} denotes the molar volume of vacant sites. The Li atoms have an occupancy $\theta \equiv N_{\mathrm{Li}}/N_{\mathrm{L}}$ and $N_{\mathrm{v}} = N_{\mathrm{L}} - N_{\mathrm{Li}}$ lattice sites are vacant, with $\theta_{\mathrm{v}} \equiv N_{\mathrm{v}}/N_{\mathrm{L}}$ denoting the fraction of these vacant sites. The internal energy is then given by

$$U_{\mathrm{m}} = \mu_0 N_{\mathrm{Li}} + h_{\mathrm{v}} N_{\mathrm{v}}, \tag{S1}$$

where h_{v} is the molar enthalpy of formation of vacant sites in Li and μ_0 is the reference molar chemical potential of the Li atoms. In writing (S1) we have assumed no contribution from the elastic energy of the Li. We neglect vibrational entropy and, therefore, set the entropy of N_{Li} moles of Li atoms, and N_{v} moles of vacant sites, equal to zero prior to mixing. Then, the entropy S_{m} of the filament is given in terms of the gas constant R by the entropy of mixing as

$$S_{\mathrm{m}} = -N_{\mathrm{L}} R[\theta \ln \theta + (1-\theta)\ln(1-\theta)]. \tag{S2}$$

The Helmholtz free-energy at temperature $T \equiv (\partial U_{\mathrm{m}}/\partial S_{\mathrm{m}})_{\Omega}$ follows as $A_{\mathrm{m}} \equiv U_{\mathrm{m}} - TS_{\mathrm{m}}$, such that

$$A_{\mathrm{m}} = \mu_0 N_{\mathrm{Li}} + h_{\mathrm{v}} N_{\mathrm{v}} + N_{\mathrm{L}}\, RT[\theta \ln \theta + (1-\theta)\ln(1-\theta)], \tag{S3}$$

and the Gibbs free-energy of the metal subjected to a pressure p (positive in compression) is $\mathcal{G}_{\mathrm{m}} \equiv A_{\mathrm{m}} + p\Omega$. The equilibrium fraction of vacant sites then follows from the condition

$$\left.\frac{\partial \mathcal{G}_{\mathrm{m}}}{\partial N_{\mathrm{L}}}\right|_{N_{\mathrm{Li}}} = 0, \tag{S4}$$

such that at $p = 0$, $\theta_{\mathrm{v}}^0 = \exp[-h_{\mathrm{v}}/(RT)]$ while at a non-zero pressure p we have $\theta_{\mathrm{v}} = \theta_{\mathrm{v}}^0 \exp[-p\Omega_{\mathrm{v}}/(RT)]$. Note that the enthalpy of formation of vacant sites in Li is $h_{\mathrm{v}} \approx 50$ kJ mol^{-1} [1]; consequently, at room temperature $T = 300$ K, we have $h_{\mathrm{v}}/(RT) \gg 1$ and therefore $\theta_{\mathrm{v}} \ll 1$ with $\theta \approx 1$. Therefore, to a high degree of accuracy $A_{\mathrm{m}} \approx \mu_0 N_{\mathrm{Li}}$.

The chemical potential of Li in the absence of an imposed pressure with an equilibrium vacancy content is given by

$$\mu_{\mathrm{Li}} \equiv \left.\frac{\partial \mathcal{G}_{\mathrm{m}}}{\partial N_{\mathrm{Li}}}\right|_{N_{\mathrm{L}}} = \mu_0, \tag{S5}$$

and the corresponding chemical potential of the Li^+ ions in the electroneutral metal is [2]

$$\mu_{\mathrm{Li}^+} = \mu_{\mathrm{Li}} - \mu_{\mathrm{el}}, \tag{S6}$$

where μ_{el} is the chemical potential of the electrons (often referred to as the Fermi level). It is reasonable to assume that the Fermi level of electrons in the electrode depends only on the electric potential φ with $\mu_{\mathrm{el}} = -F\varphi$ and thus $\mu_{\mathrm{Li}^+} = \mu_0 + F\varphi$, where F is the Faraday constant.

Now consider the chemical potential $\mu_{\mathrm{Li}^+}^{\mathrm{e}}$ of the Li^+ ions within the single-ion-conductor electrolyte. The electrolyte is assumed to remain electroneutral with every Li^+ cation paired with an immobile anion within the single-ion-conductor electrolyte. Thus, the Li^+ occupancy within the electrolyte is constant and the chemical potential of Li^+ ions within the electrolyte can be written as [2]

$$\mu_{\mathrm{Li}^+}^{\mathrm{e}} = \mu_{\mathrm{e}} + F\varphi, \tag{S7}$$

where μ_{e} is the reference chemical potential of Li^+ ions in the electrolyte and φ is the electric potential of the electrolyte. Note that there is no stress contribution to (S7) since we have

assumed that the molar volume Ω_e of Li within the electrolyte is zero [2,3] because the Li in Li-stuffed ceramic electrolytes lies within a rigid ceramic skeleton which does not deform upon removal/addition of a Li atom.

The reference quantities μ_e and μ_0 are directly related to the open circuit potential $\mathcal{U}$ of the electrode relative to the electrolyte, also known as the equilibrium potential. It is defined as the electrical potential that equalises the chemical potentials of Li^+ in the electrode and electrolyte in the absence of an external applied pressure, i.e., $\mu_0 + F\mathcal{U} = \mu_e$.

S1.2 Constitutive relations

Constitutive relations are required for the dielectric, mechanical and ion transport properties of the electrolyte. We model the electrolyte as an isotropic linear dielectric with permittivity $\mathcal{E}_{SE}$ such that the electric displacement D_i is given in terms of the electric field $E_i = -\varphi_{,i}$ by $D_i = \mathcal{E}_{SE}E_i$. The transport of Li^+ within the electrolyte is driven by the spatial gradient of the chemical potential of Li^+ that provides the driving force $f_i \equiv -\partial\mu^e_{Li^+}/\partial x_i$. The molar flux of Li^+ in the electroneutral electrolyte is $h_i \equiv mN^e_{Li^+}f_i$, where m is the mobility of Li^+ in the electrolyte and $N^e_{Li^+}$ the molar concentration of the Li^+ ions within the electrolyte. Typically, this flux is measured in terms of the current density $j_i = Fh_i$ of the Li^+ ions, with the mobility written in terms of an ionic conductivity defined as $\kappa \equiv j_1/E_1$ for an electrical field applied in the 1 −direction. Thus, setting $\kappa = mN^e_{Li^+}F^2$ shows that the current density is related to the gradient of the electric potential as $j_i = -\kappa\varphi_{,i}$ which is essentially a statement of Ohm's law. (There is no diffusive contribution to the flux as the electrolyte is assumed to remain electroneutral with fixed occupancy of Li^+ sites.) Moreover, since we are assuming an electroneutral electrolyte with a fixed concentration of Li^+ ions, conservation of Li requires that $j_{i,i} = 0$ or equivalently $\phi_{,ii} = 0$ and $D_{i,i} = 0$ since $D_i = (\mathcal{E}_{SE}/\kappa)j_i$. Finally, the electrolyte is assumed to be a linear elastic solid with shear modulus G and Poisson's ratio ν. Under small strain conditions the strain ε_{ij} is defined from the displacement field u_i as $\varepsilon_{ij} \equiv (u_{i,j} + u_{j,i})/2$ with the mechanical stress σ_{ij} then related to ε_{ij} via Hooke's law,

$$\varepsilon_{ij} = \frac{\sigma_{ij}}{2G} - \frac{\nu}{2G(1+\nu)}\sigma_{kk}\delta_{ij}, \tag{S8}$$

where δ_{ij} is the usual Kronecker delta.

In formulating the variational principle, we will also need to specify the electric fields within the Li and the empty space within the crack. We approximate the Li to be a perfect conductor with a vanishing electric field, while empty space has permittivity $\mathcal{E}_0$ which is a universal constant.

S1.3 System definition and the variational principle

Our aim is to analyse the growth of cracks and Li filaments within the electrolyte, and we thus define a system whose domain is denoted $\mathcal{V}$ and surface $\mathcal{S}$. This system excludes the external power supply but encompasses the entire electrolyte volume $\mathcal{V}_{SE}$, the Li filament and dry crack occupying volumes $\mathcal{V}_F$ and $\mathcal{V}_C$, respectively, within the electrolyte and infinitesimal layers of the electrodes as shown in Fig. S1. Correspondingly, the electrolyte has cracked surfaces $\mathcal{S}_\Gamma$

and $\mathcal{S}_{\mathrm{C}}$ where the Li filament is present and absent, respectively (Fig. S1). Thus, the system is bounded by surfaces $\mathcal{S}_{\mathrm{L}}$ and $\mathcal{S}_{\mathrm{R}}$ in the plating and stripping electrodes, respectively as well as by the top and bottom free surfaces of the electrolyte $\mathcal{S}_{\mathrm{T}}$ and $\mathcal{S}_{\mathrm{B}}$, i.e., $\mathcal{S} \equiv \mathcal{S}_{\mathrm{L}} \cup \mathcal{S}_{\mathrm{B}} \cup \mathcal{S}_{\mathrm{R}} \cup \mathcal{S}_{\mathrm{T}}$. The metal electrodes are maintained at fixed electric potentials by the external power supply while there is no flux of Li across $\mathcal{S}_{\mathrm{T}}$ and $\mathcal{S}_{\mathrm{B}}$. This sets known boundary conditions for the system being analysed. While this is the simplest system that can be analysed for investigating the growth of cracks, it is nevertheless a complex open system with fluxes of Li^+ ions across the system boundaries $\mathcal{S}_{\mathrm{L}}$ and $\mathcal{S}_{\mathrm{R}}$. In addition, there is a change in the total Li content in the system as the Li filaments grows due to Li^+ ions being deposited into the crack with a corresponding flux of electrons from the plating electrode to the filament to neutralize these Li^+ ions. While the formulation is general for simplicity of presentation, we shall describe the principle in a two-dimensional (2D) context with growth of a straight crack as depicted in Fig. S1b.

The rate of loss of a potential energy, $\dot{\Pi}$, of the system defined above drives the dissipation processes within the system as well as the fracture of the electrolyte. Let f denote the Helmholtz free-energy per unit volume of the system absent contributions from the electrical stored energy associated with the electric displacement D_i and electric field E_i within the system, while T_i are the tractions on the surface $\mathcal{S}$ of the system. At time t the crack within the electrolyte is of length a and the Li filament within the crack has a length $\zeta \leq a$ with γ_{adh} denoting the work of adhesion between the Li and the electrolyte surface and γ_{SE} the fracture energy of the electrolyte. Then within the 2D context being considered here, $\dot{\Pi}$ per unit thickness of the electrolyte given by

$$\begin{aligned}\dot{\Pi} \;=\; \int_{\mathcal{V}} \dot{f}\, d\mathcal{V} - \; & \int_{\mathcal{V}} D_i \dot{E}_i d\mathcal{V} + \frac{1}{F}\int_{\mathcal{S}_{\mathrm{R}}} \mu_{\mathrm{Li}^+} j_i n_i \, d\mathcal{S} + \frac{1}{F}\int_{\mathcal{S}_{\mathrm{L}}} \mu_{\mathrm{Li}^+} j_i n_i \, d\mathcal{S} - \int_{\mathcal{S}_{\mathrm{T}} \cup \mathcal{S}_{\mathrm{B}}} D_i n_i \dot{\varphi} d\mathcal{S} \\ & - \int_{\mathcal{S}} T_i \dot{u}_i \, d\mathcal{S} - \frac{1}{F}\int_{\mathcal{S}_{\mathrm{L}}} \mu_{\mathrm{el}} j_i^{\mathrm{el}} n_i \, d\mathcal{S} - 2\gamma_{\mathrm{adh}}\, \dot{\zeta} + \; 2\gamma_{\mathrm{SE}}\, \dot{a},\end{aligned} \tag{S9}$$

where j_i is the current density vector accounting for the flux of Li^+ ions across the electrode boundaries $\mathcal{S}_{\mathrm{R}}$ and $\mathcal{S}_{\mathrm{L}}$ within the electrodes, j_i^{el} is the current density vector accounting for the flux of electrons from the plating electrode to neutralise the charge in the Li^+ ions being deposited into the growing Li filament and n_i is the outward unit normal vector to the electrolyte. Note that in (S9) we have no boundary electrical work on $\mathcal{S}_{\mathrm{L}}$ and $\mathcal{S}_{\mathrm{R}}$ as these surfaces are just within the electrodes and held at a fixed electric potential. Now consider the first integral in (S9). The elastic energy within the solid electrolyte is given by

$$U_{\mathrm{elas}} = \int_{\mathcal{V}_{\mathrm{SE}}} w_{\mathrm{elas}} d\mathcal{V} = \frac{1}{2}\int_{\mathcal{V}_{\mathrm{SE}}} \varepsilon_{ij} \mathbb{C}_{ijkl} \varepsilon_{kl} \, d\mathcal{V}, \tag{S10}$$

where $\mathbb{C}_{ijkl} = 2G\nu\delta_{ij}\delta_{kl}/(1-2\nu) \; + G(\delta_{ik}\delta_{jl} + \delta_{il}\delta_{jk})$ is the elastic stiffness tensor and the stress $\sigma_{ij} = \mathbb{C}_{ijkl}\varepsilon_{kl}$. Noting that, other than from elasticity, there are no contributions to $\dot{f}$ from the electrolyte (that is assumed to have a fixed concentration of Li), that there are no contributions at all from the dry crack volume $\mathcal{V}_{\mathrm{C}}$ and that the infinitesimal electrode layers store negligible amount of energy, we have

$$\int_{\mathcal{V}} \dot{f}\, d\mathcal{V} = \dot{U}_{\text{elas}} + \int_{\mathcal{V}_{\text{F}}} \dot{f}\, d\mathcal{V} \tag{S11a}$$

where

$$\dot{U}_{\text{elas}} = \int_{\mathcal{V}_{\text{SE}}} \sigma_{ij} \check{\varepsilon}_{ij}\, d\mathcal{V} + U'_{\text{elas}} \dot{a}\,, \tag{S11b}$$

and

$$\check{\varepsilon}_{ij} = \left.\frac{\partial \varepsilon_{ij}}{\partial t}\right|_{a}\,, \qquad U'_{\text{elas}} = \left.\frac{\partial U_{\text{elas}}}{\partial a}\right|_{u_i n_i \in \mathcal{S}_\Gamma} \tag{S11c}$$

where the oversymbol $\check{}$ is used to denote a time derivative with the crack length held fixed. Now recall that within the assumptions discussed in Section S1.1, the rate of change of Helmholtz free-energy of the Li within the filament is well approximated by $\dot{N}_{\text{Li}}\mu_0$ where $\dot{N}_{\text{Li}}$ is the molar rate of change of the Li content in the filament. Then, with $\int_{\mathcal{V}_{\text{F}}} \dot{f}\, d\mathcal{V}$ given by $\dot{N}_{\text{Li}}\mu_0$, substitution of (S11a) into (S9) gives (1) of the main text. Upon substituting (S11a) & (S11b) into (S9) we have

$$\begin{aligned}\dot{\Pi} \;=\; & \dot{N}_{\text{Li}}\mu_0 + \int_{\mathcal{V}_{\text{SE}}} \sigma_{ij}\check{\varepsilon}_{ij}\, d\mathcal{V} - \int_{\mathcal{V}} D_i \dot{E}_i d\mathcal{V} + \frac{1}{F}\int_{\mathcal{S}_{\text{L}}} \mu_{\text{Li}^+} j_i n_i\, d\mathcal{S} + \frac{1}{F}\int_{\mathcal{S}_{\text{R}}} \mu_{\text{Li}^+} j_i n_i\, d\mathcal{S} \\ & - \int_{\mathcal{S}_{\text{T}}\cup\mathcal{S}_{\text{B}}} D_i n_i \dot{\varphi} d\mathcal{S} - \int_{\mathcal{S}} T_i \dot{u}_i\, d\mathcal{S} - \frac{1}{F}\int_{\mathcal{S}_{\text{L}}} \mu_{\text{el}} j_i^{\text{el}} n_i\, d\mathcal{S} \\ & - \left(\frac{2\gamma_{\text{adh}}}{F\rho_{\text{m}}\delta_{\text{Tip}}}\right)\left(J^{+}_{\text{Tip}} + J^{-}_{\text{Tip}}\right) + \left[U'_{\text{elas}} + 2\gamma_{\text{SE}}\right]\dot{a},\end{aligned} \tag{S12}$$

where J^{+}_{Tip} and J^{-}_{Tip} are the currents into the tip of the filament from the two crack flanks such that conservation of Li dictates that the filament extension rate

$$\dot{\zeta} = \frac{J^{+}_{\text{Tip}} + J^{-}_{\text{Tip}}}{F\rho_{\text{m}}\delta_{\text{Tip}}}, \tag{S13}$$

with δ_{Tip} the tip thickness of the Li filament (Fig. S1b) and ρ_{m} the molar density of Li metal. Without loss of generality, we set $\varphi = 0$ and $\varphi = \Phi_{\text{P}}$ as the potentials of the plating and stripping electrodes, respectively, and use the expressions for μ_{Li^+} and μ_{el} from Section S1.1 along with the conservation of Li expression

$$\int_{\mathcal{S}_{\text{L}}} j_i n_i\, d\mathcal{S} \;+\; \int_{\mathcal{S}_{\text{R}}} j_i n_i\, d\mathcal{S} \;=\; -\dot{N}_{\text{Li}} F, \tag{S14}$$

to reduce the expression (S12) for $\dot{\Pi}$ to

$$\begin{aligned}\dot{\Pi} \;=\; & \int_{\mathcal{V}_{\text{SE}}} \sigma_{ij}\check{\varepsilon}_{ij}\, d\mathcal{V} - \int_{\mathcal{V}} D_i \dot{E}_i d\mathcal{V} + \Phi_{\text{P}}\int_{\mathcal{S}_{\text{R}}} j_i n_i\, d\mathcal{S} - \int_{\mathcal{S}_{\text{T}}\cup\mathcal{S}_{\text{B}}} D_i n_i \dot{\varphi} d\mathcal{S} - \int_{\mathcal{S}} T_i \dot{u}_i\, d\mathcal{S} \\ & - \left(\frac{2\gamma_{\text{adh}}}{F\rho_{\text{m}}\delta_{\text{Tip}}}\right)\left(J^{+}_{\text{Tip}} + J^{-}_{\text{Tip}}\right) + \left[U'_{\text{elas}} \;+ 2\gamma_{\text{SE}}\right]\dot{a}.\end{aligned} \tag{S15}$$

The decrease in this potential energy is associated with dissipation in the system from: (i) flux of Li^+ through the electrolyte with an ionic conductivity κ, (ii) flux of Li^+ across the stripping and plating electrode/electrolyte interfaces $\mathcal{S}_{\text{S}}$ and $\mathcal{S}_{\text{P}}$, respectively (Fig. S1a) with a resistance Z_0, (iii) flux of Li^+ across the crack flanks $\mathcal{S}_\Gamma$ into the Li filament that is associated with a

resistance Z_f and (iv) the flux Li^+ to the Li filament tip that is associated with a tip resistance R_{Tip} (note that R_{Tip} is the resistance for the tip current while Z_f is the resistance for the flank flux and hence Z_f and R_{Tip} have different units). We then define a dissipation potential $\mathcal{D}$ for the system given by the sum of the dissipation potentials associated with each of these contributions

$$\mathcal{D} = \frac{1}{2}\left[\frac{1}{\kappa}\int_{\mathcal{V}_{\mathrm{SE}}} j_i j_i \, d\mathcal{V} + Z_0 \int_{\mathcal{S}_{\mathrm{P}}} j^2 d\mathcal{S} + Z_0 \int_{\mathcal{S}_{\mathrm{S}}} j^2 d\mathcal{S} + Z_f \int_{\mathcal{S}_{\Gamma}} j^2 d\mathcal{S} + R_{\mathrm{Tip}} \left\{\left(J^{+}_{\mathrm{Tip}}\right)^2 + \left(J^{-}_{\mathrm{Tip}}\right)^2\right\}\right], \quad \text{(S16)}$$

where $j = j_i n_i$.

Following [4-7], we define a functional $\dot{\Psi}(\check{u}_i, \dot{\varphi}, j_i, J^{\pm}_{\mathrm{Tip}}, \dot{a})$

$$\dot{\Psi} = \dot{\Pi} + \mathcal{D}, \quad \text{(S17)}$$

and the system evolves such that $\dot{\Psi}$ is stationary with respect to arbitrary variations in the kinetic variables $(\check{u}_i, \dot{\varphi}, j_i, J^{+/-}_{\mathrm{Tip}}, \dot{a})$, i.e., $\delta\dot{\Psi} = 0$. We shall consider the variations of $\delta\dot{\Pi}$ and $\delta\mathcal{D}$ separately. Taking the variation of (S15) and applying divergence theorem we obtain

$$\begin{aligned}\delta\dot{\Pi} = \Phi_{\mathrm{P}} \int_{\mathcal{S}_{\mathrm{R}}} \delta j_i n_i \, d\mathcal{S} - \int_{\mathcal{V}} D_{i,i}\delta\dot{\varphi} d\mathcal{V} - \int_{\mathcal{V}_{\mathrm{SE}}} \sigma_{ij,j}\delta\check{u}_i d\mathcal{V} + \int_{\mathcal{S}_{\Gamma}} \tilde{T}_i \delta\check{u}_i \, d\mathcal{S} \\ - \left(\frac{2\gamma_{\mathrm{adh}}}{F\rho_{\mathrm{m}}\delta_{\mathrm{Tip}}}\right)\left(\delta J^{+}_{\mathrm{Tip}} + \delta J^{-}_{\mathrm{Tip}}\right) + \left[U'_{\mathrm{elas}} + 2\gamma_{\mathrm{SE}}\right]\delta\dot{a}.\end{aligned} \quad \text{(S18)}$$

where $\tilde{T}_i$ on $\mathcal{S}_{\Gamma}$ is the traction applied on the solid electrolyte by the filament. In writing (S18) we have noted that the tractions on the surfaces $\mathcal{S}_S \cup \mathcal{S}_P$ of the electrolyte in contact with the electrodes vanish as do tractions on $\mathcal{S}_{\mathrm{L}} \cup \mathcal{S}_{\mathrm{R}} \cup \mathcal{S}_{\mathrm{T}} \cup \mathcal{S}_{\mathrm{B}}$. Moreover, the electrolyte has cracked surfaces $\mathcal{S}_{\Gamma}$ and $\mathcal{S}_{\mathrm{C}}$ where the Li filament is present and absent, respectively, and the tractions vanish on $\mathcal{S}_{\mathrm{C}}$, and thus only the surface integral of tractions over $\mathcal{S}_{\Gamma}$ remains in (S18). This expression can be further simplified by recalling that the electric field and therefore D_i vanishes within the infinitesimal electrode layers and Li filament while within the electrolyte $D_{i,i} = 0$ since $D_i = (\mathcal{E}_{\mathrm{SE}}/\kappa) j_i$ and electroneutrality of the electrolyte requires $j_{i,i} = 0$. Thus, since $D_{i,i} = 0$ in $\mathcal{V} \setminus \mathcal{V}_{\mathrm{C}}$, the volume integral over $\mathcal{V}$ in (S18) reduces to an integral over the volume $\mathcal{V}_{\mathrm{C}}$ of empty space within the crack and (S18) can be written as

$$\begin{aligned}\delta\dot{\Pi} = \Phi_{\mathrm{P}} \int_{\mathcal{S}_{\mathrm{R}}} \delta j_i \, n_i \, d\mathcal{S} - \int_{\mathcal{V}_{\mathrm{C}}} D_{i,i}\delta\dot{\varphi} d\mathcal{V} - \int_{\mathcal{V}_{\mathrm{SE}}} \sigma_{ij,j}\delta\check{u}_i d\mathcal{V} + \int_{\mathcal{S}_{\Gamma}} T_n \delta\check{u}_n \, d\mathcal{S} \\ - \left(\frac{2\gamma_{\mathrm{adh}}}{F\rho_{\mathrm{m}}\delta_{\mathrm{Tip}}}\right)\left(\delta J^{+}_{\mathrm{Tip}} + \delta J^{-}_{\mathrm{Tip}}\right) + \left[U'_{\mathrm{elas}} + 2\gamma_{\mathrm{SE}}\right]\delta\dot{a}\,,\end{aligned} \quad \text{(S19)}$$

where we have assumed that the shear tractions vanish on $\mathcal{S}_{\Gamma}$ with $T_n = -\sigma_{ij} n_j n_i = -\sigma_n$ and $u_n = -u_i n_i$ being the normal tractions and displacements, respectively. Note that T_n and u_n both have positive senses that are in the direction of the inward normal to the electrolyte. Therefore, T_n provides the algebraic value of the crack opening tractions on the crack surfaxes and $2u_n$ is the algebraic value of the crack opening displacements. Finally, recall that U'_{elas} is calculated with u_n fixed on the crack flanks $\mathcal{S}_{\Gamma}$. Thus, Li conservation dictates that the Li flux is related to the crack opening via $\dot{u}_n = \check{u}_n = j_i n_i/(F\rho_{\mathrm{m}})$ and (S19) is then rewritten as

$$\delta\dot{\Pi} = \Phi_{\mathrm{P}} \int_{\mathcal{S}_{\mathrm{R}}} \delta j_i n_i \, d\mathcal{S} - \int_{\mathcal{V}_{\mathrm{C}}} D_{i,i}\delta\dot{\varphi} d\mathcal{V} - \int_{\mathcal{V}_{\mathrm{SE}}} \sigma_{ij,j}\delta\dot{u}_i d\mathcal{V} - \frac{1}{F\rho_{\mathrm{m}}}\int_{\mathcal{S}_{\Gamma}} \sigma_n \delta j_i \, n_i d\mathcal{S} - \left(\frac{2\gamma_{\mathrm{adh}}}{F\rho_{\mathrm{m}}\delta_{\mathrm{Tip}}}\right)\left(\delta J^{+}_{\mathrm{Tip}} + \delta J^{-}_{\mathrm{Tip}}\right) + [U'_{\mathrm{elas}} + 2\gamma_{\mathrm{SE}}]\delta\dot{a} \, . \tag{S20}$$

Now consider the variation of the dissipation potential (S16). Recalling that $j_i = -\kappa\varphi_{,i}$ and $j_{i,i} = 0$ in $\mathcal{V}_{\mathrm{SE}}$, application of the divergence theorem to the integral over $\mathcal{V}_{\mathrm{SE}}$ gives the variation $\delta\mathcal{D}$ as

$$\delta\mathcal{D} = -\int_{\mathcal{S}_{\mathrm{SE}}} (\varphi + \varphi_0)\delta j_k n_k d\mathcal{S} + Z_0 \int_{\mathcal{S}_{\mathrm{P}}} j_i n_i \, \delta j_k n_k \, d\mathcal{S} + Z_0 \int_{\mathcal{S}_{\mathrm{S}}} j_i n_i \, \delta j_k n_k \, d\mathcal{S} + Z_f \int_{\mathcal{S}_{\Gamma}} j_i n_i \, \delta j_k n_k \, d\mathcal{S} + R_{\mathrm{Tip}}\left(J^{+}_{\mathrm{Tip}}\delta J^{+}_{\mathrm{Tip}} + J^{-}_{\mathrm{Tip}}\delta J^{-}_{\mathrm{Tip}}\right), \tag{S21}$$

where φ_0 is a constant of integration that we will specify subsequently and $\mathcal{S}_{\mathrm{SE}} \equiv \mathcal{S}_{\mathrm{P}} \cup \mathcal{S}_{\Gamma} \cup \mathcal{S}_{\mathrm{C}} \cup \mathcal{S}_{\mathrm{B}} \cup \mathcal{S}_{\mathrm{S}} \cup \mathcal{S}_{\mathrm{T}}$ is the surface of $\mathcal{V}_{\mathrm{SE}}$ (Fig. S1a and b). The fluxes $j_i n_i$ vanish of the top and bottom surfaces $\mathcal{S}_{\mathrm{T}}$ and $\mathcal{S}_{\mathrm{B}}$ of the electrolyte as well as on the crack surface $\mathcal{S}_{\mathrm{C}}$ where there is no Li filament, and these reduce (S21) to

$$\delta\mathcal{D} = \int_{\mathcal{S}_{\mathrm{P}}} [Z_0 j_i n_i - (\varphi + \varphi_0)]\delta j_k n_k \, d\mathcal{S} + \int_{\mathcal{S}_{\mathrm{S}}} [Z_0 j_i n_i - (\varphi + \varphi_0)]\delta j_k n_k \, d\mathcal{S} + \int_{\mathcal{S}_{\Gamma}} \left[Z_f j_i n_i - (\varphi + \varphi_0)\right]\delta j_k n_k \, d\mathcal{S} + \left[R_{\mathrm{Tip}}J^{+}_{\mathrm{Tip}} - \left(\varphi^{+}_{\mathrm{Tip}} + \varphi_0\right)\right]\delta J^{+}_{\mathrm{Tip}} + \left[R_{\mathrm{Tip}}J^{-}_{\mathrm{Tip}} - \left(\varphi^{-}_{\mathrm{Tip}} + \varphi_0\right)\right]\delta J^{-}_{\mathrm{Tip}}, \tag{S22}$$

where we have used the fact that the flux at the Li filament tip located at ζ is singular but its integral over $\mathcal{S}_{\Gamma}$ around the Li filament tip is finite such that

$$J^{\pm}_{\mathrm{Tip}} = \lim_{\epsilon\to 0}\int_{\zeta-\epsilon}^{\zeta+\epsilon} j^{\pm}_i n^{\pm}_i d\Gamma, \tag{S23}$$

with $j^{\pm}_i$ and $n^{\pm}_i$ denoting the fluxes and the electrolyte outward unit normal on the two crack flanks and Γ the path along the Li filament/electrolyte interface. In (S22) $\varphi^{\pm}_{\mathrm{Tip}}$ is the electric potential in the electrolyte adjacent to the Li filament tip located at ζ.

Given that the electrode layers within the system are infinitesimal, $j_i n_i$ on $\mathcal{S}_{\mathrm{S}}$ equals that on $\mathcal{S}_{\mathrm{R}}$. Using this continuity requirement, combining (S20) and (S22), and setting $\delta\dot{\Psi} = \delta\dot{\Pi} + \delta\mathcal{D} = 0$ we find

$$\begin{aligned}\delta\dot{\Psi} = &-\int_{\mathcal{V}_{\mathrm{C}}} D_{i,i}\delta\dot{\varphi} d\mathcal{V} - \int_{\mathcal{V}_{\mathrm{SE}}} \sigma_{ij,j}\delta\dot{u}_i d\mathcal{V} + \int_{\mathcal{S}_{\mathrm{S}}} [\Phi_{\mathrm{P}} - (\varphi + \varphi_0) + Z_0 j_i n_i] \, \delta j_k n_k \, d\mathcal{S} \\ &+ \int_{\mathcal{S}_{\mathrm{P}}} [-(\varphi + \varphi_0) + Z_0 j_i n_i] \, \delta j_k n_k \, d\mathcal{S} \\ &+ \int_{\mathcal{S}_{\Gamma}} \left[-(\varphi + \varphi_0) - \frac{\sigma_n}{F\rho_{\mathrm{m}}} + Z_f j_i n_i\right] \delta j_k n_k \, d\mathcal{S} \\ &+ \left[-\left(\frac{2\gamma_{\mathrm{adh}}}{F\rho_{\mathrm{m}}\delta_{\mathrm{Tip}}}\right) - \left(\varphi^{+}_{\mathrm{Tip}} + \varphi_0\right) + R_{\mathrm{Tip}}J^{+}_{\mathrm{Tip}}\right]\delta J^{+}_{\mathrm{Tip}} \\ &+ \left[-\left(\frac{2\gamma_{\mathrm{adh}}}{F\rho_{\mathrm{m}}\delta_{\mathrm{Tip}}}\right) - \left(\varphi^{-}_{\mathrm{Tip}} + \varphi_0\right) + R_{\mathrm{Tip}}J^{-}_{\mathrm{Tip}}\right]\delta J^{-}_{\mathrm{Tip}} + [U'_{\mathrm{elas}} + 2\gamma_{\mathrm{SE}}]\delta\dot{a} = 0.\end{aligned} \tag{S24}$$

Since $(\delta\dot{u}_i, \delta\dot{\varphi}, \delta j_i, \delta J^{\pm}_{\mathrm{Tip}}, \delta\dot{a})$ are arbitrary it follows that $\sigma_{ij,j} = 0$ in $\mathcal{V}_{\mathrm{SE}}$ which is the usual stress equilibrium equation that has boundary conditions $T_i = 0$ on all $\mathcal{S}_{SE}$ except the crack flanks $\mathcal{S}_{\Gamma}$. On $\mathcal{S}_{\Gamma}$ only the shear tractions vanish while the normal displacement rate is given by

$\dot{u}_n = j_i n_i/(F\rho_{\mathrm{m}})$. Moreover, the crack length is set by the "Griffith condition" that emerges from (S24), viz.

$$U'_{\mathrm{elas}} = \left.\frac{\partial U_{\mathrm{elas}}}{\partial a}\right|_{u_i n_i \in \mathcal{S}_\Gamma} = -2\gamma_{\mathrm{SE}}\,. \tag{S25}$$

Within the electrolyte $\mathcal{V}_{\mathrm{SE}}$ the requirement that $j_{i,i} = 0$ implies that the electric potential needs to satisfy $\varphi_{,ii} = 0$. The boundary conditions of this Laplace equation follow from (S24), viz., $j_i n_i = 0$ on $\mathcal{S}_{\mathrm{T}}$, $\mathcal{S}_{\mathrm{B}}$ and $\mathcal{S}_{\mathrm{C}}$ implying we have the Neuman boundary condition $\varphi_{,i} n_i = 0$ on these surfaces. On the surfaces where there is a Li^+ flux $j_i n_i = -\kappa\varphi_{,i} n_i$, (S24) dictates the Robin boundary conditions

$$j_i n_i \;=\; \frac{\varphi + \varphi_0 - \Phi_{\mathrm{P}}}{Z_0} \quad \text{on} \quad \mathcal{S}_{\mathrm{S}}, \tag{S26}$$

$$j_i n_i \;=\; \frac{\varphi + \varphi_0}{Z_0} \quad \text{on} \quad \mathcal{S}_{\mathrm{P}}, \tag{S27}$$

$$j_i n_i = \frac{1}{Z_f}\left(\varphi + \varphi_0 + \frac{\sigma_n}{F\rho_{\mathrm{m}}}\right) \quad \text{on} \quad \mathcal{S}_\Gamma, \tag{S28}$$

and

$$J^{\pm}_{\mathrm{Tip}} \;=\; \frac{1}{R_{\mathrm{Tip}}}\left[\varphi^{\pm}_{\mathrm{Tip}} + \varphi_0 + \left(\frac{2\gamma_{\mathrm{adh}}}{F\rho_{\mathrm{m}}\delta_{\mathrm{Tip}}}\right)\right]. \tag{S29}$$

Finally, (S24) requires that $D_{i,i} = -\mathfrak{E}_0\varphi_{,ii} = 0$ in $\mathcal{V}_{\mathrm{C}}$. The boundary conditions for this Laplace equation are $D_i n_i = 0$ on the surface of $\mathcal{V}_{\mathrm{C}}$ so that there is no jump in the normal electric displacement at the interface of $\mathcal{V}_{\mathrm{C}}$ with the electrolyte and Li filament and thereby no charge build-up at these interfaces. Thus, the electric potential, field and displacement vanish throughout $\mathcal{V}_{\mathrm{C}}$.

It now remains to specify the integration constant φ_0. We consider the case with no crack and the two electrodes subject to the same potential (which without loss of generality is $\Phi_{\mathrm{P}} = 0$). Under these conditions there is no Li^+ flux in the electrolyte so that the electric potential φ within the electrolyte is spatially uniform and boundary conditions (S26) and (S27) then require $\varphi = -\varphi_0$. Thus, the constant of integration is the open circuit potential $\mathcal{U}$, i.e., $\varphi_0 = \mathcal{U}$ and it is convenient to rewrite the governing equations and boundary conditions for the electrical/transport problem in terms of a shifted potential $\hat{\varphi} \equiv \varphi + \mathcal{U}$. The governing equation for $\hat{\varphi}$ in $\mathcal{V}_{\mathrm{SE}}$ is $\hat{\varphi}_{,ii} = 0$ with boundary conditions

$$j_i n_i \;=\; \frac{\hat{\varphi} - \Phi_{\mathrm{P}}}{Z_0} \quad \text{on} \quad \mathcal{S}_{\mathrm{S}}, \tag{S30}$$

$$j_i n_i \;=\; \frac{\hat{\varphi}}{Z_0} \quad \text{on} \quad \mathcal{S}_{\mathrm{P}}, \tag{S31}$$

$$j_i n_i = \frac{1}{Z_f}\left(\hat{\varphi} + \frac{\sigma_n}{F\rho_{\mathrm{m}}}\right) \quad \text{on} \quad \mathcal{S}_\Gamma, \tag{S32}$$

and

$$J_{\mathrm{Tip}}^{\pm} = \frac{1}{R_{\mathrm{Tip}}}\left[\hat{\varphi}_{\mathrm{Tip}}^{\pm} + \left(\frac{2\gamma_{\mathrm{adh}}}{F\rho_{\mathrm{m}}\delta_{\mathrm{Tip}}}\right)\right]. \tag{S33}$$

This is coupled with the mechanical governing equation $\sigma_{ij,j} = 0$ in $\mathcal{V}_{\mathrm{SE}}$ with traction-free boundary conditions on all surfaces except $\mathcal{S}_{\Gamma}$ where we specify the crack flank displacement rate $\dot{u}_n = j_i n_i/(F\rho_{\mathrm{m}})$ and vanishing shear tractions. Finally, the crack length is given by the Griffith condition (S25), while the filament length is given by the evolution equation (S13). This completes the variational principle which delivers the governing equations and the associated boundary conditions.

S2. Numerical solution methodology

The above variational principle provides strongly coupled mechanical and electrochemical balance laws and associated boundary conditions. Before discussing the methodology for the numerical solution of these equations we shall first discuss the method used to regularise the governing equation $\hat{\varphi}_{,ii} = 0$ in $\mathcal{V}_{\mathrm{SE}}$ which has a singularity associated with the current into the tip of the Li filament.

The solutions presented in the main body of the paper are for plane strain 2D crack growth with the crack growing perpendicular to the plating electrode/electrolyte interface and located at the mid-plane of the electrolyte (Fig. 2). The problem is thus symmetric about the crack plane and in the following we shall describe the solution methodology for this symmetric case where the fluxes across both crack flanks are equal and $J_{\mathrm{Tip}}^{-} = J_{\mathrm{Tip}}^{+}$ as well as $\hat{\varphi}_{\mathrm{Tip}}^{+} = \hat{\varphi}_{\mathrm{Tip}}^{-}$. We shall thus refer to these quantities simply as J_{Tip} and $\hat{\varphi}_{\mathrm{Tip}}$ with the crack propagating along $x_2 = 0$ and the crack and filament tips located at $(a, 0)$ and $(\zeta, \pm\delta_{\mathrm{Tip}}/2)$, respectively.

S2.1 Superposition methodology for the solution of the Laplace equation in the electrolyte

The sink at the Li filament tip creates computational difficulties in terms of a direct numerical solution and here we propose a superposition method for solving $\hat{\varphi}_{,ii} = 0$ along with the interface conditions (S30-S33). In 2D, the electric potential at a radius r from the filament tip, due to a line sink (along the x_3 −direction in Fig. S1) of strength $\mathcal{C}$ in an infinite medium is

$$\tilde{\varphi}(r) = \mathcal{C}\ln(2r/\delta_{\mathrm{Tip}}). \tag{S34}$$

Here we have normalised (S34) such that $\tilde{\varphi} = 0$ at $r = \delta_{\mathrm{Tip}}/2$ which is taken to be the filament tip, i.e., $\tilde{\varphi}_{\mathrm{Tip}} = 0$. The potential field (S34) satisfies $\tilde{\varphi}_{,ii} = 0$ for $r > 0$, but also results in a current flux into the filament tip. The current flux $\tilde{J}_{\mathrm{Tip}}$ per unit thickness of the electrolyte into the tip (where the current into the tip is defined as positive) associated with this potential field is readily calculated by considering a circular contour $\mathcal{R}$ centred at $r = 0$. The flux across unit length of this contour is $\tilde{j}_i\tilde{n}_i$, where $\tilde{n}_i$ is the unit outward normal to the contour and $\tilde{j}_i =$

$-\kappa\tilde{\varphi}_{,i}$. Since $\tilde{\varphi}_{,ii} = 0$ for $r > 0$, this flux represents the flux into the sink located at $r = 0$ and follows as

$$2\tilde{J}_{\text{Tip}} = -\int_{\mathcal{R}} \tilde{\jmath}_i \tilde{n}_i d\Gamma = \kappa \int_{\mathcal{R}} \frac{\partial \tilde{\varphi}}{\partial r} d\Gamma = 2\pi\kappa\mathcal{C}. \tag{S35}$$

so that $\tilde{J}_{\text{Tip}} = \pi\kappa\mathcal{C}$. Note that the field $\tilde{\varphi}$ gives a current flux into the filament tip, but it does not satisfy all boundary conditions on $\mathcal{V}_{\text{SE}}$; imposition of these boundary conditions along with (S33) will set the value of $\tilde{J}_{\text{Tip}}$ via the value obtained for $\mathcal{C}$.

In order to satisfy the required boundary conditions, we recall linearity of the Laplace equation $\hat{\varphi}_{,ii}$ and write the potential within the electrolyte as $\hat{\varphi} = \breve{\varphi} + \tilde{\varphi}$. Recalling that $\tilde{\varphi}_{,ii} = 0$, the solution of the total potential field reduces to solving $\breve{\varphi}_{,ii} = 0$ with the appropriate boundary conditions. These boundary conditions in terms of $\breve{\jmath}_i = -\kappa\breve{\varphi}_{,i}$ are:

(i) The Neumann boundary conditions that enforce zero flux across the boundaries with free-space, viz. $\breve{\varphi}_{,2} = -\tilde{\varphi}_{,2}$ along $x_2 = \pm W/2$ and the crack flank where the Li filament is absent, viz. ($\zeta < x_1 < a$ along $x_2 = 0$). Note that $\tilde{\varphi}_{,2} = 0$ on $x_2 = 0$ so on $\zeta < x_1 < a$ along $x_2 = 0$ the boundary condition reduces to $\breve{\varphi}_{,2} = 0$.

(ii) The Robin boundary conditions for the linearized Butler-Volmer flux relations along the electrode/electrolyte interfaces, viz.

$$\breve{\jmath}_1 = \frac{\breve{\varphi} + \tilde{\varphi} - \Phi_{\text{P}}}{Z_0} + \kappa\tilde{\varphi}_{,1} \quad \text{on} \quad \mathcal{S}_{\text{S}} \ (x_1 = L), \tag{S36}$$

and

$$-\breve{\jmath}_1 = \frac{\breve{\varphi} + \tilde{\varphi}}{Z_0} - \kappa\tilde{\varphi}_{,1} \quad \text{on} \quad \mathcal{S}_{\text{P}} \ (x_1 = 0). \tag{S37}$$

(iii) Robin-like boundary conditions for flux along the upper crack flank where the Li filament is present, viz. along $\mathcal{S}_\Gamma$ ($0 < x_1 < \zeta$ on $x_2 = 0$)

$$-\breve{\jmath}_2 = \frac{1}{Z_f}\left(\breve{\varphi} + \tilde{\varphi} + \frac{\sigma_n}{F\rho_{\text{m}}}\right). \tag{S38}$$

The numerical solution of this boundary value problem for a given applied Φ_{P} furnishes the distribution $\breve{\varphi}(x_1, x_2)$ within the electrolyte for an assumed value of $\mathcal{C}$ and known σ_n and the filament tip overpotential follows as $\hat{\varphi}_{\text{Tip}} = \breve{\varphi}_{\text{Tip}}(\mathcal{C}) = \breve{\varphi}_{\text{Tip}}(x_1 = \zeta, x_2 = \delta_{\text{Tip}}/2)$ since $\tilde{\varphi}_{\text{Tip}} = 0$.

It remains to determine $\mathcal{C}$ using (S33). The total current into the filament tip is $J_{\text{Tip}} = \breve{J}_{\text{Tip}} + \tilde{J}_{\text{Tip}}$, where $\breve{J}_{\text{Tip}}$ is the current due to the $\breve{\varphi}$ field. Considering a circular contour centred at the filament tip and using the divergence theorem, it follows that $\breve{J}_{\text{tip}} = 0$ since $\breve{\varphi}$ is a smooth field that satisfies $\breve{\varphi}_{,ii} = 0$. Then combining (S33) and (S35) we obtain

$$\mathcal{C} = \frac{1}{\pi\kappa R_{\text{Tip}}}\left[\breve{\varphi}_{\text{Tip}}(\mathcal{C}) + \frac{2\gamma_{\text{adh}}}{F\rho_{\text{m}}\delta_{\text{Tip}}}\right], \tag{S39}$$

giving an implicit relation for $\mathcal{C}$.

S2.2 Numerical computation algorithm

We employ a staggered algorithm to solve the coupled electro-mechanical boundary value problem for the Li filament and crack propagation using a time step Δt. The solution is calculated using the Lagrangian finite element partial differential equation solver in the

COMSOL Multiphysics package in a two-dimensional plane strain setting. We used 4-node quadrilateral elements with linear interpolation functions. The quadrilateral size is ~ $0.1\mu m \times 0.1\mu m$ in the vicinity of the entire crack flank and over the crack path along $x_2 = 0$. The mesh is gradually coarsened towards the top and bottom boundaries $\mathcal{S}_T$ and $\mathcal{S}_B$. In all the simulations we employed a time increment $\Delta t = (i_{Ref}/i_\infty)25$ ms, where the reference current density is $i_{Ref} = 1.0$ mA cm^{-2}. Mesh and time step convergence studies were performed to confirm the adequacy of these numerical parameters.

Given the solution (i.e., all field variables) at time t we first solve for the overpotential $\hat{\varphi}$ at time $t + \Delta t$ in $\mathcal{V}_{SE}$ governed by the Laplace equation $\hat{\varphi}_{,ii} = 0$ and the boundary conditions (S30 – S33). As per the staggered algorithm, the interface stress, σ_n in (S32), is taken from the known solution at time t. However, recall that the solution of $\hat{\varphi}_{,ii} = 0$ as discussed in section S2.1 involves determining of the strength $\mathcal{C}$ of the Li filament tip sink. Thus, the boundary value problem (BVP) for $\hat{\varphi}_{,ii} = 0$ with the known tractions is solved iteratively (see Eq. S39) to determine $\mathcal{C}$ and thereby the potential field $\hat{\varphi} = \breve{\varphi} + \tilde{\varphi}$ and the filament tip current given by

$$J_{Tip} = \frac{1}{R_{Tip}}\left[\breve{\varphi}_{Tip} + \left(\frac{2\gamma_{adh}}{F\rho_m\delta_{Tip}}\right)\right], \tag{S40}$$

where we use $\delta_{Tip} = 5$ nm. Next, we update the filament length via $\zeta(t + \Delta t) = \zeta(t) + \Delta t\dot{\zeta}$ where

$$\dot{\zeta} = \begin{cases} \dfrac{2J_{Tip}}{F\rho_m\delta_{Tip}} & \text{if } \zeta(t+\Delta t) \le a \\ \dfrac{a-\zeta}{\Delta t} & \text{otherwise.} \end{cases}, \tag{S41}$$

The crack opening displacement $\delta_{Li}(x_1, t + \Delta t) = 2u_n(x_1, t + \Delta t)$ over the filament length ζ is then calculated as

$$\delta_{Li}(x_1, t + \Delta t) = \delta_{Li}(x_1, t) + \frac{2j_f}{F\rho_m}\Delta t, \tag{S42}$$

where $j_f = j_i n_i$ is given by (S32) over the filament length.

Given now the solution of $\hat{\varphi}_{,ii} = 0$ we solve the mechanical BVP $\sigma_{ij,j} = 0$ in $\mathcal{V}_{SE}$ with the known crack opening displacements (S42) over the filament length and traction-free boundary conditions on all other surfaces (as well as shear traction-free conditions on the crack flanks in contact with the filament) to provide the mechanical fields at time $t + \Delta t$. This solution is performed keeping the crack length a held fixed. To determine the crack length we now calculate one half of the crack tip J-integral on semi-circular contours $\mathcal{R}$ of radius R centered at the crack tip via

$$-\frac{1}{2}\frac{\partial U_{elas}}{\partial a} = \mathcal{J}_I = \int_{\mathcal{R}}\left[w_{elas}m_1 - m_j\sigma_{ji}\frac{\partial u_i}{\partial x_1}\right] d\mathcal{R} + \frac{1}{2}\int_{a-R}^{a}\sigma_n\frac{\partial\delta}{\partial x_1}\, dx_1, \tag{S43}$$

where m_i is the outward unit normal to $\mathcal{R}$, we have augmented the usual J-integral to account for the non-zero crack flank tractions, and we recall that σ_n is the tensile stress across the interface between the electrolyte and the filament. If $\mathcal{J}_I > \gamma_{SE}$ we release one node of the finite element mesh ahead of the crack tip and the mechanical BVP is resolved leading to further crack growth until $\mathcal{J}_I \le \gamma_{SE}$, providing the full solution at time $t + \Delta t$ for all the field variables, viz. (u_i, φ, ζ, a).

S3: Modification of variational principle and numerical solution technique when debonding between filament and crack flanks is permitted

The variational principle and associated numerical solution methodology have assumed that the crack opening over the region where the Li filament is present is given by the Li flux with no constraints on the crack flank tractions T_n. These tractions can thus become tensile and thus we have effectively assumed that adhesion between the Li and electrolyte crack flanks is sufficiently strong that the interface can sustain arbitrary tensile tractions. A more realistic condition is that the interface can sustain no tensile tractions and we are required to implement the constraint $\sigma_n \leq 0$ with γ_{adh} set equal to zero, where we recall that σ_n is the tensile stress across the interface.

The variational principle and all associated equations and boundary conditions outlined in Section S1.3 do not change but rather an additional constitutive constraint of $\sigma_n \leq 0$ is added. This constraint means that the crack flanks can detach from the Li filament and hence over the region within the crack where the Li filament exists (i.e., $0 \leq x_1 \leq \zeta, x_2 = 0$) the crack opening displacement $\delta \geq \delta_{\mathrm{Li}}$ where

$$\dot{\delta}_{\mathrm{Li}}(x_1, t) = \begin{cases} \dfrac{2j_f}{F\rho_{\mathrm{m}}} & 0 \leq x_1 \leq \zeta, \\ 0 & \text{otherwise.} \end{cases} \tag{S44}$$

The mechanical BVP is then solved via an interactive "contact" type algorithm such that if the solution gives $\sigma_n \leq 0$ we use a displacement boundary condition $\delta = \delta_{\mathrm{Li}}$ at that location along the filament. Otherwise, we allow for debonding to occur such that $T_n = 0$ and the crack opening $\delta > \delta_{\mathrm{Li}}$ emerges from the solution of the mechanical BVP.

Supplementary References

[1] H. Schultz, *Mater. Sci. Eng.* **1991**, A141, 149-167.
[2] S. S. Shishvan, N. A. Fleck, R. M. McMeeking, V. S. Deshpande, *J. Power Sources*, **2020**, 456, 227989.
[3] M. Klinsmann, F. E. Hildebrand, M. Ganser, R. M. McMeeking, *J. Power Sources*, **2019**, 422, 227226.
[4] L. Onsager, *Phys. Rev.* **1931**, 37, 405-426.
[5] L. Onsager, *Phys. Rev.* **1931**, 38, 2265-2279.
[6] Z. Suo, *Adv. App. Mech.*, **1997**, 33, 193-294.
[7] A.C.F. Cocks, S.P.A. Gill, J. Pan, *Adv. App. Mech.*, **1998**, 36, 81-162.

Supplementary Figures

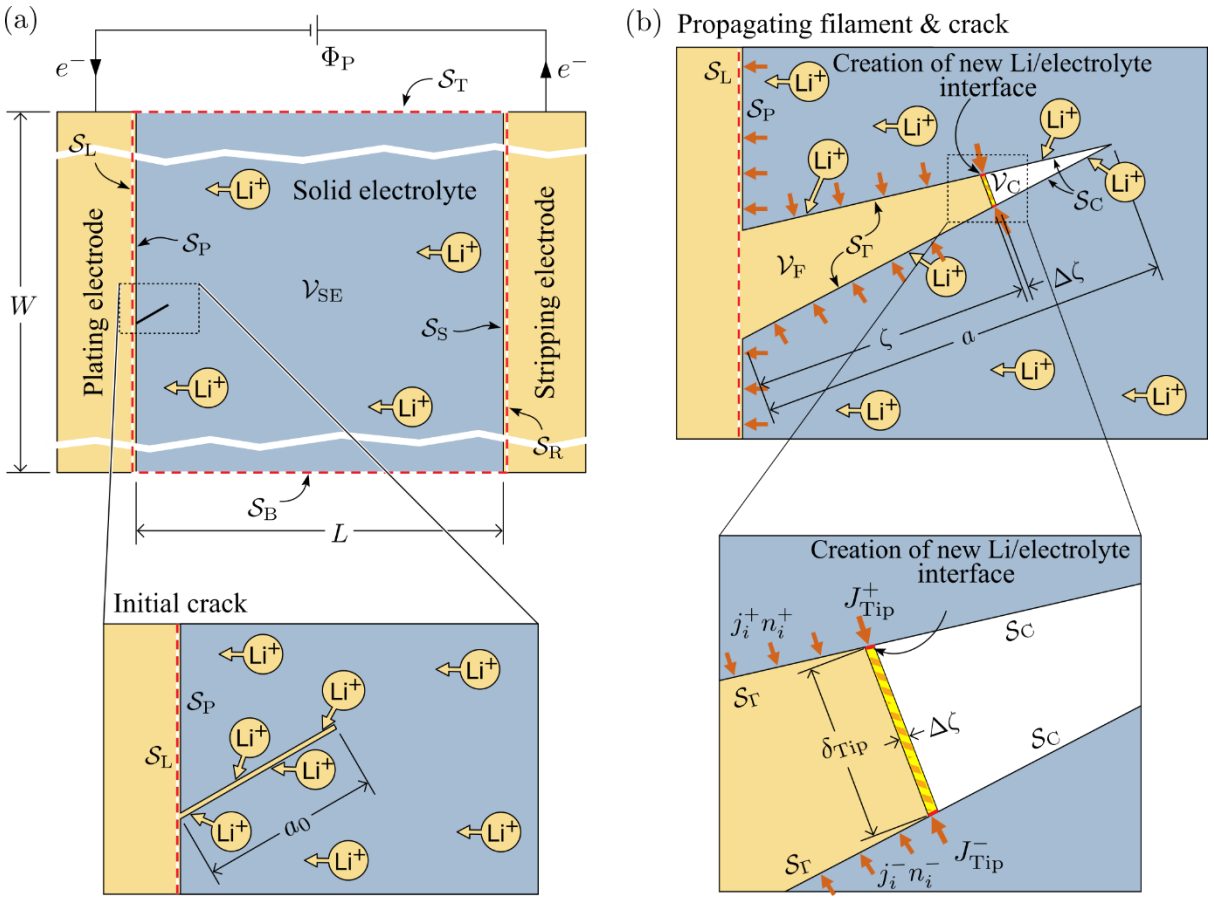

Figure S1: (a) Sketch of the symmetric Li/electrolyte/Li cell along with the inset showing the initial crack of length a_0 that emerges from the boundary with the plating electrode (see inset). The system analysed is of volume $\mathcal{V}$ and is bounded by the top and bottom surfaces of the electrolyte $\mathcal{S}_T$ and $\mathcal{S}_B$, respectively and the left and right boundaries $\mathcal{S}_L$ and $\mathcal{S}_R$, respectively that lie just within the plating and stripping electrodes. The stripping and plating electrolyte/electrode boundaries are denoted by $\mathcal{S}_S$ and $\mathcal{S}_P$, respectively. (b) Sketch showing a zoom-in of the propagating crack and Li filament of length a and ζ, respectively. The interface between the electrolyte and Li filament is denoted by $\mathcal{S}_\Gamma$ while the flanks of the crack where the filament is absent is identified as $\mathcal{S}_C$. The volume of the filament and dry crack are denoted by $\mathcal{V}_F$ and $\mathcal{V}_C$, respectively, so that $\mathcal{V} \equiv \mathcal{V}_{SE} \cup \mathcal{V}_F \cup \mathcal{V}_C$ plus the infinitesimal layers of the electrodes included in the system. A zoomed view of the filament tip shows the fluxes into the filament from the top and bottom interfaces having unit outward normals n_i^+ and n_i^- (pointing out of the electrolyte). The currents into the top and bottom of the crack tip responsible for the Li filament propagation are indicated as J^+_{Tip} and J^-_{Tip}, respectively.

Supplementary Videos

Supplementary Video S1: Temporal evolution of the normalised flux $\hat{j} \equiv \sqrt{j_i j_i}/i_\infty$ (along with a quiver plot to show the direction of the flux within the electrolyte) and stress σ_{22} within the electrolyte having initial crack of length $a_0 = 25\mu\text{m}$ for the cell with $R_{\text{Tip}} = 0$ and loaded by a current $i_\infty = 1\ \text{mAcm}^{-2}$. Debonding of the Li from the crack flanks is not permitted. The opening of the crack is magnified $\times 200$ so that the crack profile is clearly visible.

Supplementary Video S2: Temporal evolution of the normalised flux $\hat{j} \equiv \sqrt{j_i j_i}/i_\infty$ (along with a quiver plot to show the direction of the flux within the electrolyte) and stress σ_{22} within the electrolyte having initial crack of length $a_0 = 25\mu\text{m}$ for the cell with $R_{\text{Tip}} = 0$ and loaded by a current $i_\infty = 1\ \text{mAcm}^{-2}$. Debonding between the Li filament and crack flanks is assumed to occur such that the crack flank tractions $T_n \geq 0$. The opening of the crack is magnified $\times 200$ so that the crack profile is clearly visible.

Supplementary Video S3: Temporal evolution of the normalised flux $\hat{j} \equiv \sqrt{j_i j_i}/i_\infty$ (along with a quiver plot to show the direction of the flux within the electrolyte) and stress σ_{22} within the electrolyte for the cell with $R_{\text{Tip}} = 22\ \Omega\text{cm}$ and loaded by a current $i_\infty = 1\ \text{mAcm}^{-2}$. Debonding is assumed to occur such that the crack flank tractions $T_n \geq 0$. The opening of the crack is magnified $\times 200$ so that the crack profile is clearly visible. The crack tip in this case outruns the Li filament.